ADVANCING EARTH AND SPACE SCIENCES

JGR Solid Earth

RESEARCH ARTICLE
10.1029/2025JB033674

# Earthquake Populations From Stochastic Stress Fields

**Gregory C. McLaskey**[1], **David S. Kammer**[2], **and Chun-Yu Ke**[3]

[1]Department of Civil and Environmental Engineering, Cornell University, Ithaca, NY, USA, [2]Institute for Building Materials, ETH Zurich, Zurich, Switzerland, [3]Department of Civil Engineering, National Taiwan University, Taipei, Taiwan

**Key Points:**

- We represent the heterogeneous stresses produced by slip on rough faults with a stochastic stress field defined by statistical parameters
- Realistic earthquake populations occur when the stress field is highly variable and alternates between positive and negative values
- Populations from highly variable stress fields match multiple characteristics of natural earthquakes including b-value and stress drop

**Supporting Information:**

Supporting Information may be found in the online version of this article.

**Correspondence to:**

G. C. McLaskey,
gcm8@cornell.edu

**Citation:**

McLaskey, G. C., Kammer, D. S., & Ke, C.-Y. (2026). Earthquake populations from stochastic stress fields. *Journal of Geophysical Research: Solid Earth*, *131*, e2025JB033674. https://doi.org/10.1029/2025JB033674

Received 19 DEC 2025
Accepted 27 JUN 2026

**Author Contributions:**

**Conceptualization:** Gregory C. McLaskey
**Data curation:** Gregory C. McLaskey
**Formal analysis:** Gregory C. McLaskey
**Investigation:** Gregory C. McLaskey
**Methodology:** Gregory C. McLaskey
**Resources:** Gregory C. McLaskey
**Software:** Gregory C. McLaskey
**Validation:** Gregory C. McLaskey
**Visualization:** Gregory C. McLaskey
**Writing – original draft:** Gregory C. McLaskey
**Writing – review & editing:** Gregory C. McLaskey, David S. Kammer, Chun-Yu Ke



## Abstract

Earthquakes occur in populations with few large events and many small ones, yet many earthquake rupture models employ a smooth stress field and other conditions that prohibit the co-occurrence of large earthquakes and smaller foreshocks and aftershocks. We describe populations of earthquakes that propagate and arrest within a stochastic stress field $\Delta\tau_{\mathrm{pot}}(x)$ using a 1D fracture mechanics framework. $\Delta\tau_{\mathrm{pot}}(x)$ is characterized by its mean ($mean_{\Delta\tau}$), standard deviation ($stdev_{\Delta\tau}$), and scaling exponent ($m_{\Delta\tau}$), which describes how $\Delta\tau_{\mathrm{pot}}(x)$ changes as a function of wavelength. $\Delta\tau_{\mathrm{pot}}(x)$ is related to the strain energy that fuels earthquakes, and it embodies the heterogeneous stresses that develop in fault zones with multi-scale geometrical complexity. Realistic populations of earthquakes, with more small ones than large ones, are produced by highly variable fields with $stdev_{\Delta\tau}$ (8–80 MPa) that far exceeds $mean_{\Delta\tau}$, resulting in significant sections with highly negative $\Delta\tau_{\mathrm{pot}}(x)$. Earthquake populations produced by such variable stress fields exhibit b-values that decrease with increasing $mean_{\Delta\tau}$ and stress drops that are primarily correlated with $stdev_{\Delta\tau}$, are independent of magnitude, and may be limited by the strength of rocks at seismogenic depths. Our preferred models suggest $0 \leq m_{\Delta\tau} \leq 0.25$ ($m_{\Delta\tau} = 1.5$ is self-similar, 1.0 is Brownian, 0 is white noise), consistent with expectations based on multiscale roughness measured on exhumed faults. This suggests that $\Delta\tau_{\mathrm{pot}}(x)$ must be highly variable and highly negative, even at short wavelengths, a property that strongly influences the earthquake energy budget but is absent from state-of-the-art dynamic rupture models and unresolvable with kinematic finite-fault inversions.

## Plain Language Summary

Geologists describe faults that slip during earthquakes as highly complex features, with geometric irregularities that include bumps, jogs, stepovers, and a waviness at a variety of length scales. However, seismologists and those who study the mechanics of earthquakes tend to simplify faults as planar structures with nearly constant properties. Modern computer simulations of large earthquakes can reproduce some of their characteristics such as their permanent ground deformation and aspects of their shaking, but fail to reproduce measured foreshocks and aftershocks and do not even allow for populations of earthquakes with a variety of sizes. This work describes a modeling framework that specifically acknowledges the complex features of real fault zones by making fault properties variable in space. This model is used to explore how much variability is needed to produce a variety of earthquake sizes. We find that the energy stored in the crust that fuels earthquakes and causes them to grow must be highly variable in space and even negative in many locations. This means that earthquakes do not rupture smoothly or continuously but in an erratic way where they suddenly begin and may nearly stop multiple times as they grow and eventually die out.

## 1. Introduction

Earthquakes rupture faults that are not planar and instead have a complex architecture (e.g., Mitchell & Faulkner, 2009) that is known to affect how earthquakes nucleate (Dodge et al., 1995) and where earthquake ruptures slow down or stop (Gabrieli & Tal, 2025; Rodriguez Padilla et al., 2024). Earthquake rupture simulations can reproduce many aspects of earthquake behavior, but even state-of-the-art dynamic rupture simulations (e.g., Ando & Kaneko, 2018; Harris et al., 2021; Ulrich et al., 2019) often employ a relatively smooth stress field and other conditions that may be inconsistent with the multi-scale roughness observed on natural faults (Brown & Scholz, 1985; Candela et al., 2012; Renard et al., 2006; Sagy et al., 2007). Such models have difficulty producing both large **M**7 earthquakes and smaller **M**1 to **M**3 foreshocks and aftershocks and are thus inconsistent with a fundamental observation: earthquakes occur in populations with few large events and many small ones. This work uses a physics-based modeling framework to identify the conditions where such populations of earthquakes result naturally.

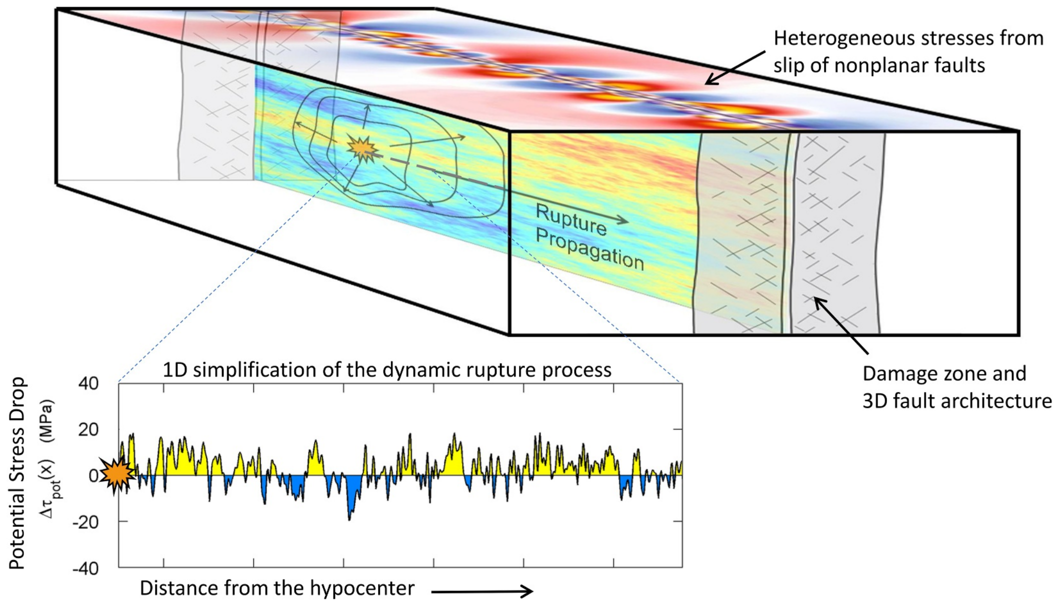


**Figure 1.** Conceptual framework for simplifying the complex architecture of a fault zone and the heterogeneous stresses that develop with slip into a rupture propagating along a 1-dimensional stochastic stress field. Adapted from Dieterich and Smith (2009) and Mitchell and Faulkner (2009).

Classical theories of earthquake mechanics assumed that relevant properties such as stress, strength, and fracture energy were constants (e.g., Andrews, 1976; Brune, 1970; Madariaga, 1976). Numerical simulations of dynamic ruptures along rough faults (e.g., Dunham et al., 2011; Heimisson, 2020; Shi & Day, 2013; Tal & Hager, 2018) are computationally expensive, so limited cases have been explored. Other studies have implemented spatially variable properties to acknowledge the effects of fault roughness/architecture without modeling fault roughness directly. These include variable shear stress (e.g., Ampuero et al., 2006; Andrews, 1980; Smith & Heaton, 2011) or variable fracture energy (e.g., Albertini et al., 2021; Ide & Aochi, 2005; Renou et al., 2022; Venegas- Aravena et al., 2024). When coupled with nonlinear dependencies present in earthquake mechanics, spatial variability of some parameters can produce transformative and unexpected behavior; however, a comprehensive understanding of those effects is still lacking.

In this study, we vary the parameter $\Delta\tau_{pot}$, which depends on both stress and strength, but leave others constant. Sometimes referred to as "effective stress," "dynamic stress drop," or "stress drop potential function" (Hanks, 1979) $\Delta\tau_{pot} = \tau_0 - \tau_r$ is defined as the initial shear stress level $\tau_0$ relative to the fault's residual sliding strength $\tau_r$ (Andrews, 1980; Dempsey & Suckale, 2016). Potential stress drop $\Delta\tau_{pot}$ is a measure of the strain energy that can be accessed to provide fuel for an earthquake. It has been shown to strongly influence a number of earthquake properties, such as rupture velocity and the transition to supershear rupture (Andrews, 1976) as well as seismological stress drop (Brune, 1970). In laboratory earthquake experiments, it has been shown to control earthquake rupture propagation and arrest (e.g., Bayart et al., 2016; Dong et al., 2023; Ke et al., 2018).

An alternative end-member model would be to treat fracture energy as variable and $\Delta\tau_{pot}$ as constant. In Section 5, we describe how variability in $\Delta\tau_{pot}$ can be replaced by variability in fracture energy in some circumstances. However, the current study focuses on variable $\Delta\tau_{pot}$ since observations such as reverse-polarity earthquake pairs (e.g., Shearer et al., 2024), borehole breakout stress orientation (e.g., Barton & Zoback, 1994), and spatially variable fault slip (e.g., Manighetti et al., 2001) point toward variable stress along faults (Smith & Heaton, 2011, and references therein).

Figure 1 depicts how multi-scale geometrical complexity and the heterogeneous stresses that develop within fault zones are idealized as the spatially varying field $\Delta\tau_{pot}(x, y, z)$. Building on previous efforts (Ampuero et al., 2006; Dempsey et al., 2016; Dempsey & Suckale, 2016; Ripperger et al., 2007), we analyze populations of earthquakes produced by 1-dimensional fields $\Delta\tau_{pot}(x)$ and extract features of those populations that are likely to be relevant to natural earthquakes despite the extreme simplification of the model. However, previous efforts assumed that earthquakes initiate according to a nucleation criterion, and we assume that they initiate abruptly and at random locations, which we argue is justified for sufficiently rough fault zones, as described in Section 3.2 and Section 6.3.

The Gutenberg-Richter law (Gutenberg & Richter, 1944) indicates that earthquakes exist at a wide range of sizes, and there are more small earthquakes than large ones. This work aims to determine the conditions on $\Delta\tau_{\mathrm{pot}}(x)$ needed to approximately adhere to the Gutenberg-Richter law. We also consider the earthquake stress drop $\Delta\sigma$ and how $\Delta\sigma$ changes with earthquake size. By matching characteristics of our simulated earthquake populations to those found among naturally occurring earthquakes, we provide constraints on the statistics of $\Delta\tau_{\mathrm{pot}}(x)$, which may, in turn, provide insight into the underlying physics of earthquakes and fault zones.

## 2. Modeling Approach

### 2.1. Potential Stress Drop $\Delta\tau_{\mathrm{pot}}(x)$ and Its Relationship to Fault Roughness

Potential stress drop $\Delta\tau_{\mathrm{pot}}(x)$ can likely be linked to the architecture of a fault zone. When considering a single fault, a relevant quantity is fault roughness (i.e., fault topography $u(x)$), which can be measured in the lab and on exhumed fault surfaces (Brodsky et al., 2016; Brown & Scholz, 1985; Candela et al., 2012; Power et al., 1987; Renard et al., 2006; Sagy et al., 2007). Fault architecture can also be inferred at depth using high precision earthquake locations (Cochran et al., 2023). These studies have found that fault roughness is self-affine, and further specifics are discussed in Sections 2.3 and 6.2. In general, we might imagine that very rough or immature faults or complex fault zones that consist of a variety of misoriented faults have highly variable stress and strength and therefore highly variable $\Delta\tau_{\mathrm{pot}}(x)$. In contrast, smooth and mature faults might have smoother $\Delta\tau_{\mathrm{pot}}(x)$.

Recent studies have linked fault roughness to fault stresses (Cattania & Segall, 2021; Romanet et al., 2020, 2024; Wise & Tal, 2024) that develop when rough faults slip. Shear stress variations are proportional to the slope of the roughness,

$$\tau_0(x) \propto d(u(x))/dx, \tag{1}$$

and effective normal stress variations are proportional to the curvature of the roughness

$$\sigma_N(x) \propto d^2(u(x))/dx^2. \tag{2}$$

We expect $\Delta\tau_{\mathrm{pot}}(x)$ to be most similar to the slope of fault roughness, but, because it depends on both stress and strength, it may also be influenced by the curvature if $\tau_r = \mu_r\sigma_N$, where $\mu_r$ is a dynamic friction coefficient (e.g., Okubo & Dieterich, 1984). The above expressions give guidance for the expected properties of $\Delta\tau_{\mathrm{pot}}(x)$ with respect to fault roughness. However, fault zones likely cannot be characterized by fault roughness alone and depend on the thickness of gouge layers, damage zones, and perhaps other factors such as time-dependent slip and relaxation processes (Sirorattanakul et al., 2025; Sone & Uchide, 2016).

### 2.2. Parameters That Define $\Delta\tau_{\mathrm{pot}}(x)$

This work sets aside the difficult problem of relating $\Delta\tau_{\mathrm{pot}}(x)$ to fault zone architecture and instead studies the characteristics of earthquake ruptures that propagate and arrest within a stochastic field $\Delta\tau_{\mathrm{pot}}(x)$ defined by four parameters:

1. $mean_{\Delta\tau}$, the average value of $\Delta\tau_{\mathrm{pot}}(x)$,
2. $stdev_{\Delta\tau}$, the standard deviation of $\Delta\tau_{\mathrm{pot}}(x)$,
3. $m_{\Delta\tau}$, describes how $\Delta\tau_{\mathrm{pot}}(x)$ changes as a function of wavelength, and
4. $\lambda_{\min\Delta\tau,}$ the minimum wavelength, related to the cutoff frequency of $\Delta\tau_{\mathrm{pot}}(x)$.

Approximate adherence to the Gutenberg-Richter law (Gutenberg & Richter, 1944) places constraints on these four parameters that appear to be consistent with fault roughness measurements and the strength of the brittle crust. Other common earthquake observations, such as scale-invariant 1–10 MPa stress drops and b-values that decrease with increasing stress, are produced by the model without precise tuning.

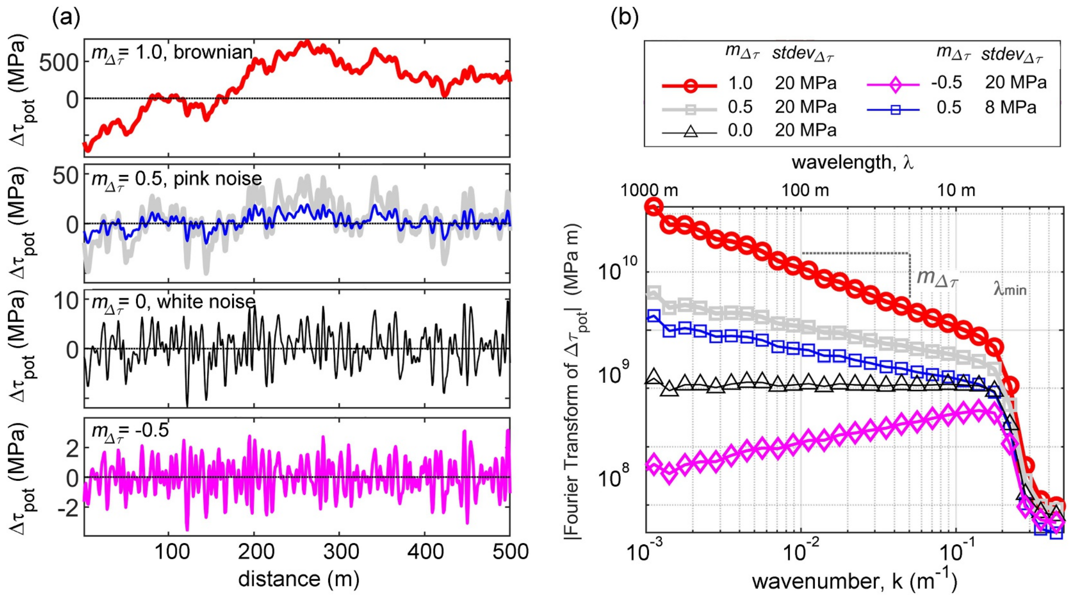


**Figure 2.** Examples of self-affine random fields $\Delta\tau_{pot}(x)$ across which earthquake ruptures propagate and arrest. (a) Spatial distribution of $\Delta\tau_{pot}(x)$ for various $m_{\Delta\tau}$. (b) The amplitude of the Fourier transform of the fields in (a) show the effect of $m_{\Delta\tau}$ and $\lambda_{\min\Delta\tau}$ in the spectral (wavenumber) domain and how differences in $stdev_{\Delta\tau}$ equate to offsets in the spectral domain. Fields with larger $m_{\Delta\tau}$ have stronger long-wavelength components.

### 2.3. Hurst Exponent and $m_{\Delta\tau}$

Figure 2 describes the parameter $m_{\Delta\tau}$, which is the slope of the Fourier transform of $\Delta\tau_{pot}(x)$ on a log-log plot. The equivalent parameter for fault roughness, $m_u$, is related to the Hurst exponent ($m_u = H+0.5$) and the slope $\alpha$ of the power spectral density ($m_u = \alpha/2$) (Beeler, 2023). In general, $\Delta\tau_{pot}(x)$ is assumed to be a self-affine random field, but if $m_{\Delta\tau} = 1.5$, then it is self-similar. $m_{\Delta\tau} = 1$ for Brownian (random walk), $m_{\Delta\tau} = 0.5$ for pink noise, and $m_{\Delta\tau} = 0$ for white noise. Figure 2a shows example stress fields for $m_{\Delta\tau}$ ranging from $-0.5$ to 1.0 while Figure 2b shows the absolute value of their Fourier transforms in the wavenumber domain. Higher $m_{\Delta\tau}$ causes large-amplitude long-wavelength features, while smaller $m_{\Delta\tau}$ reduces that drift and enhances the contribution of short-wavelength features.

## 3. Simulation Methodology

### 3.1. Creation and Parametrization of $\Delta\tau_{pot}(x)$

Realizations of $\Delta\tau_{pot}(x)$ are created from white noise $\tau_{rand}(x)$, which is a sequence of $n$ random numbers pulled from a uniform distribution. This can be considered the stress distribution along a fault of length $n\Delta x$ that is discretely sampled every $\Delta x$. Then we Fourier transform that sequence into the spectral domain (wavenumber domain)

$$T_{rand}(k) = \int_{-\infty}^{\infty} \tau_{rand}(x)\, e^{-i2\pi kx} dx \tag{3}$$

where $k$ is the (ordinary) wavenumber, the inverse of the wavelength (i.e., $k = 1/\lambda$). We apply the Fourier transform using the Fast Fourier Transform (fft) algorithm in MATLAB. A sequence of random numbers makes white noise ($m_{\Delta\tau} = 0$), so we then apply a scale factor $k^{-m}$ to change the spectral characteristics of $\tau_{rand}(x)$ to match the desired $m_{\Delta\tau}$. An inverse Fourier transform is used to return to the spatial domain:

$$\Delta\tau_{pot}^{unscaled}(x) = \int_{-\infty}^{\infty} k^{-m_{\Delta\tau}} T_{rand}(k)\, e^{i2\pi kx} dk. \tag{4}$$

10.1029/2025JB033674

We then low-pass filter $\Delta\tau_{pot}^{unscaled}(x)$ with a cutoff frequency $k_{max} = 1/\lambda_{min}$, and scale and offset $\Delta\tau_{pot}^{unscaled}(x)$ by the desired standard deviation and mean, respectively, to produce a realization of $\Delta\tau_{pot}(x)$ with a specified mean $mean_{\Delta\tau}$, standard deviation $stdev_{\Delta\tau}$, spectral falloff $m_{\Delta\tau}$, and minimum wavelength $\lambda_{min\Delta\tau}$.

### 3.2. Rupture Initiation Criterion

A key difference between this study and previous work is in the rupture initiation process. This work assumes that dynamic ruptures simply initiate at the left edge of the domain; thus, the initiation location is not correlated with $\Delta\tau_{pot}(x)$ and parameters such as $mean_{\Delta\tau}$ can be prescribed arbitrarily. Previous work assumed that ruptures initiated when and where local stress exceeded some peak strength according to a Coulomb failure criterion (Dempsey & Suckale, 2016) or nucleation process (Ampuero et al., 2006; Ripperger et al., 2007) characterized by a nucleation length scale $L_c$ (e.g., Albertini et al., 2021; Uenishi & Rice, 2003). This forces rupture to initiate from particular features of $\Delta\tau_{pot}(x)$, such as its maximum value, if $\tau_r$ is constant, and prevents $mean_{\Delta\tau}$ from being set arbitrarily. This complicates and potentially biases the model results, particularly since current earthquake nucleation models are based on faults with nearly uniform properties that neglect the contributions from fault roughness/architecture that are central to the current work.

With the random initiation employed in this study, ruptures will immediately arrest if they happen to initiate in a fault section where $\Delta\tau_{pot}(x) < 0$. For those that do find favorable stress conditions, the fracture mechanics framework for rupture propagation, described below, implicitly assumes that ruptures are immediately dynamic, without a slow nucleation phase. This implies that $L_c$ is smaller than $\Delta x$, that a crack-like rupture quickly develops, and that the size of the process zone quickly becomes small enough to warrant a small-scale yielding approximation (e.g., Kammer et al., 2024). Section 6.3 describes how random initiation on rough faults may still be consistent with a Coulomb failure criterion and presents evidence from natural earthquakes that support a small $L_c$.

### 3.3. Fracture Mechanics Framework for Rupture Propagation

Rupture propagation follows a simplified fracture mechanics model of a one-dimensional rupture, similar to previous efforts (Ampuero et al., 2006; Dempsey & Suckale, 2016; Ripperger et al., 2007). This simplification of the rupture process has been shown to encapsulate the main dependency on $\Delta\tau_{pot}(x)$ and compares favorably with fully dynamic 3D simulations (Ampuero et al., 2006). This study considers only unilateral ruptures that initiate on the left side of the domain and propagate to the right. As the ruptures advance, the rupture propagation velocity $C_{Rupt}$ can be approximated (Svetlizky et al., 2017) by comparing the fracture energy $\Gamma_{tot}$ to the static energy release rate $G_0$

$$C_{Rupt}(x) \approx \left(1 - \frac{\Gamma_{tot}(x)}{G_0(x)}\right) C_{Rayl}, \tag{5}$$

where $C_{Rayl}$, is the Rayleigh wave velocity.

### 3.4. Strain Energy Release Rate $G_0$

$G_0$ is a measure of the strain energy fueling the rupture (e.g., Freund, 1998). $G_0 \geq G_{dyn}$, since the dynamic energy release rate $G_{dyn}$ excludes energy radiated away from the rupture front as seismic waves. $G_0(x)$ is a nonlocal quantity and a nonlinear function of $(\Delta\tau_{pot}(x)^2)$. It is related to the static stress intensity factor $K_0$ via

$$G_0(x) = K_0(x)^2/E', \tag{6}$$

where, for plane strain, $E' = E/(1\text{-}\nu^2)$, and $E$ and $\nu$ are the Young's modulus and Poisson's ratio of the material, respectively. $K_0(x)$ depends both on $\Delta\tau_{pot}(x)$ and the geometry of the problem; for example, for an edge crack in an infinite elastic medium (Tada et al. (2000), Equation 5.10 and 8.3),

$$K_0(s) = \frac{2}{\sqrt{\pi a}} \int_0^a \Delta\tau_{pot}(s) \frac{F(s/a)}{\sqrt{(1 - s/a)^2}} ds, \tag{7}$$

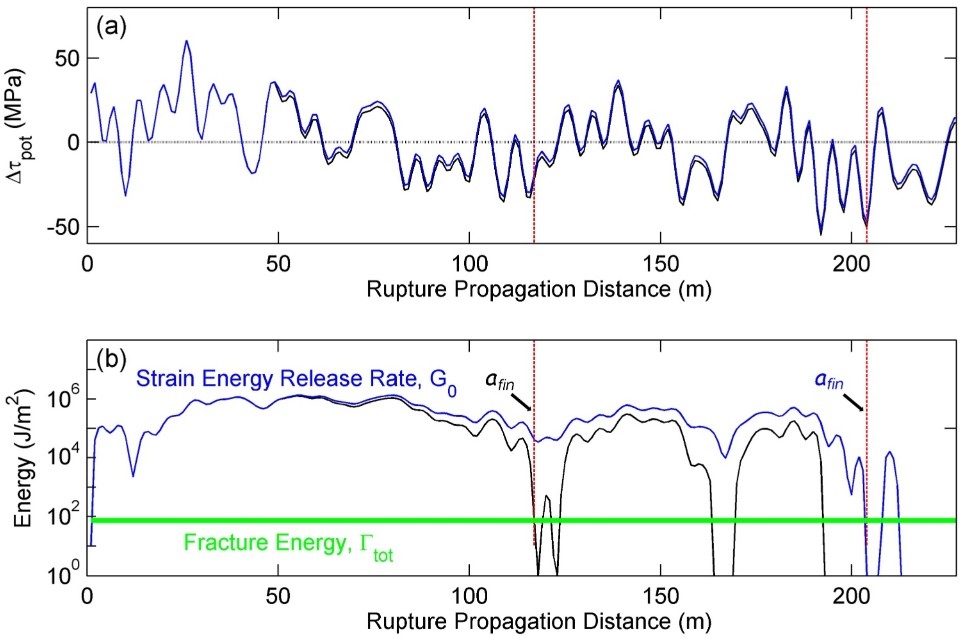


**Figure 3.** Connection between $\Delta\tau_{pot}(x)$ and rupture propagation. (a) Examples of highly variable $\Delta\tau_{pot}(x)$ and (b) corresponding strain energy release rate $G_0$ calculated from Equation 6 and Equation 7. Small differences in $\Delta\tau_{pot}(x)$ (blue vs. black lines, see text) cause large differences in $G_0$ that affect the rupture arrest location $a_{fin}$, defined as the location where $G_0$ falls below fracture energy $\Gamma_{tot}$ (green line).

where $F(s/a) = 1.297 - 0.297(s/a)^{5/4}$. Similar formulations can be derived for other geometries. For simplicity, Equation 7 is used here.

### 3.5. Fracture Energy

$\Gamma_{tot}(x)$ is the fracture energy required to advance a rupture front and includes energy dissipation associated with breaking frictional contacts, fracturing intact rock, and off-fault damage processes that occur near the rupture front (Kammer et al., 2024), but it excludes "heat" which is defined as the energy associated with sliding the fault surfaces at their residual frictional shear strength level $\tau_r$. We assume

$$\Gamma_{tot} = \gamma\sigma_N, \tag{8}$$

as found previously for both rocks (Brodsky et al., 2020; Wong, 1986) and polymers (Bayart et al., 2016, 2018), where $\gamma$ is a fracture energy coefficient and $\sigma_N$ is effective normal stress. For most of this work, we assume that $\Gamma_{tot} = 75$ J/m$^2$, which suggests that $\gamma = 0.5$ μm and $\sigma_N = 150$ MPa at seismogenic depths. However, in Section 5, we vary $\Gamma_{tot}$ and show that (a) results are insensitive to variations in $\Gamma_{tot}$ as long as $\Delta\tau_{pot}(x)$ is highly variable and (b) variation in $\Delta\tau_{pot}(x)$ can be replaced by variation in $\Gamma_{tot}(x)$ in some circumstances.

### 3.6. Rupture Arrest Criterion

If the rupture front encounters large $\Delta\tau_{pot}(x)$ or small $\Gamma_{tot}(x)$, it will have a tendency to accelerate, and when a rupture encounters low or negative $\Delta\tau_{pot}(x)$ or very high $\Gamma_{tot}(x)$, it will have a tendency to decelerate (Equation 5). Note that negative $\Delta\tau_{pot}(x)$ need not imply that the fault experiences an opposite sense of shear stress, it simply means that the strength $\tau_r$ exceeds the shear stress $\tau_0$. Figure 3a shows examples of $\Delta\tau_{pot}(x)$ and Figure 3b illustrates corresponding $G_0(x)$, determined from Equation 7 and Equation 6. Negative $\Delta\tau_{pot}(x)$ causes dramatic reductions in $G_0(x)$. $\Gamma_{tot} = 75$ J/m$^2$ and is plotted in green in Figure 3b. If

$$G_0(x) < \Gamma_{tot}(x), \tag{9}$$

then the rupture will arrest with final rupture length $a_{\text{fin}}$. The example in Figure 3 shows that small changes in $\Delta\tau_{\text{pot}}(x)$ can change $G_0(x)$ by orders of magnitude and affect the location of rupture arrest. The blue line in Figure 3a shows a $\Delta\tau_{\text{pot}}(x)$ that is 3 MPa greater than the black line for $x \geq 50$ m. This higher $\Delta\tau_{\text{pot}}(x)$ causes rupture to arrest at $x = 204$ m (blue line in Figure 3b) rather than $x = 117$ m (black line).

### 3.7. Earthquake Parameters Derived From Simulations

For a rupture that arrests at location $x = a_{\text{fin}}$, where $a_{\text{fin}}$ is smaller than the domain size $n\Delta x$, we calculate a simplified stress drop

$$\Delta\sigma^{\text{simp}} = \frac{1}{a_{\text{fin}}}\int_0^{a_{\text{fin}}} (\Delta\tau_{\text{pot}}(x))\,dx \tag{10}$$

as the average of $\Delta\tau_{\text{pot}}$ over the rupture length. Previous studies calculated stress drops $\Delta\sigma$ weighted by an assumed elliptical slip distribution (Ampuero et al., 2006; Dempsey & Suckale, 2016; Ripperger et al., 2007). For simplicity, Equation 10 is adopted here, since it has minor effects on the results.

We then assume that $a_{\text{fin}}$ is the radius of a circular rupture and calculate a simplified seismic moment

$$\mathrm{M}_0^{\text{simp}} = {a_{\text{fin}}}^3 * \Delta\sigma^{\text{simp}}. \tag{11}$$

The magnitude **M** of the earthquakes is determined from $\mathbf{M} = 2/3 \cdot \log_{10}(\mathrm{M_0}^{\text{simp}}) – 6.067$ (Hanks & Kanamori, 1979). Note that previous studies determined a 2D seismic moment of the form $\mathrm{M_0}^{2\mathrm{D}} \propto {a_{\text{fin}}}^2 * \Delta\sigma$ which is seismic moment per unit of out-of-plane length and has units of Newtons rather than Newton-meters (Ampuero et al., 2006; Dempsey & Suckale, 2016; Ripperger et al., 2007). The choice of $\mathrm{M}_0$ formulation does systematically effect some population parameters. For example, the b-value determined from $\mathrm{M_0}^{\text{simp}}$ (Equation 11) will be 0.667 times the b-value calculated from $\mathrm{M_0}^{2\mathrm{D}}$, and stress drop scaling, described below, will be similarly affected.

### 3.8. Population Parameters

We generate a population of $N$ ruptures that initiate on the left side of the domain and propagate to the right along $N$ realizations of $\Delta\tau_{\text{pot}}(x)$ generated from specified parameters: $mean_{\Delta\tau}$, $stdev_{\Delta\tau}$, $m_{\Delta\tau}$, $\lambda_{\min\Delta\tau}$. As mentioned previously, many of the ruptures are "dead on arrival" and satisfy the arrest criterion (Equation 9) at $x = 0$. Some ruptures never arrest and propagate across the entire domain. The rest of the ruptures propagate and arrest to produce a distribution of rupture lengths $a_{\text{fin}}$ and stress drops $\Delta\sigma^{\text{simp}}$ and thus a distribution of magnitudes **M**, as shown in Figure 4. We then organize ruptures by their size and determine the average $\Delta\sigma^{\text{simp}}$ four each group, shown as yellow filled symbols in Figure 4c. From this, we determine two population parameters: the average stress drop of a **M** 3 earthquake ($\Delta\sigma_{\mathbf{M3}}$, described further below) and stress drop scaling (i.e., 0.2 MPa/**M**). We also determine the b-value from the slope of a Gutenberg-Richter magnitude-frequency relation, shown in Figure 4b. For these parameters, we divided the events into four groups per magnitude unit since it yielded reasonably smooth distributions, given the number of events in the populations, which ranged from $N = 1{,}000$ to $N = 50{,}000$ (Tables S1–S2 in Supporting Information S1).

For the calculation of stress drop scaling and b-value, we only utilize a "usable magnitude range" between $\mathrm{M_0}^{\text{lowerlimit}}$ (shown as a red vertical line in Figure 4) and $\mathrm{M_0}^{\text{upperlimit}}$ (blue and black vertical dotted lines in Figure 4). The upper limit is defined as the largest magnitude bin that contains at least one rupture smaller than the total domain size, $n\Delta x$. The lower limit is set to exclude small ruptures with a size that is not significantly larger than discretization $\Delta x$. Thus, properties of the ruptures are not strongly affected by the discreteness of rupture initiation. $\mathrm{M_0}^{\text{lowerlimit}} = {a_{\min}}^3 \cdot \Delta\sigma^{\text{assumed}}$, where $a_{\min} = 100 \cdot \Delta x$, and $\Delta\sigma^{\text{assumed}} = 1$ MPa. For our parameters, $\mathrm{M_0}^{\text{lowerlimit}}$ is **M** ∼2. For the simulations considered in this work, $n = 10{,}000$, $\Delta x = 1$ m, so that maximum magnitude is **M** ∼6. We only report parameters from populations with a "usable magnitude range" of more than one magnitude unit. With this $\mathrm{M_0}^{\text{lowerlimit}}$ and minimum range, the parameter $\Delta\sigma_{\mathbf{M3}}$ was used because **M** 3 was the largest earthquake that would be in the usable magnitude range for all populations reported in Table S1 in Supporting Information S1.

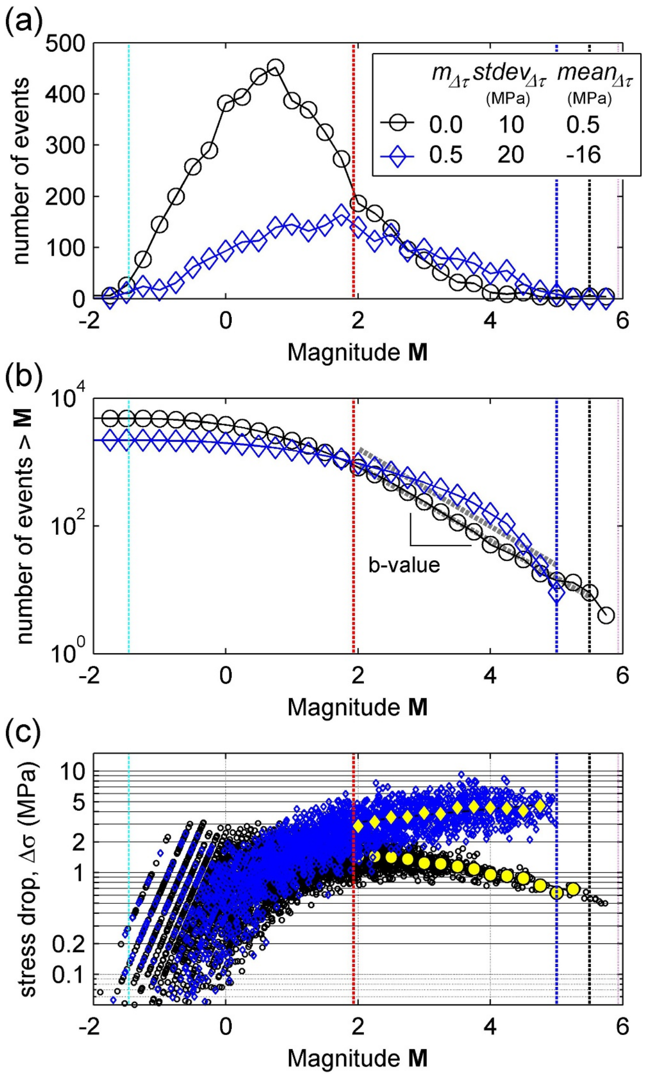


**Figure 4.** Examples of earthquake populations generated from two different statistical descriptions of $\Delta\tau_{pot}(x)$. Compared to the $m_{\Delta\tau} = 0$ population (black), the $m_{\Delta\tau} = 0.5$ population (blue) has higher $\Delta\sigma$ because it has a higher $stdev_{\Delta\tau}$. Both populations have similar b-values of 0.6 (slope of the gray dotted lines in (b)). However, the $m_{\Delta\tau} = 0.5$ population shows convexity of the magnitude-frequency distribution, which is a departure from the log-linear shape reported in natural earthquake populations. Both populations were generated from 20,000 realizations of $\Delta\tau_{pot}$(x), though about 50% and 75% of the $m_{\Delta\tau} = 0.0$ and $m_{\Delta\tau} = 0.5$ cases, respectively, were “dead on arrival” and failed to produce a rupture of finite size. Neither population produced a single rupture that failed to arrest.

## 4. Results

### 4.1. Stress Drop Primarily Depends on $stdev_{\Delta\tau}$

One of the clearest results is that stress drop is strongly affected by the $stdev_{\Delta\tau}$, with minor dependencies on other parameters. Stress drop is the average $\Delta\tau_{pot}(x)$ over the rupture area and denoted $\Delta\sigma^{simp}$ (Equation 10) for an individual simulated earthquake and denoted $\Delta\sigma_{\mathbf{M}3}$ when it describes a population of earthquakes derived from one statistical description of $\Delta\tau_{pot}(x)$. As shown in Figure 5, stress drop can largely be approximated

$$\Delta\sigma_{\mathbf{M}3} = stdev_{\Delta\tau}/C_{\sigma}, \tag{12}$$

where $C_{\sigma}$ is a constant. Populations with $m_{\Delta\tau} = 0$ are well characterized by $C_{\sigma} = 8$, while populations with positive $m_{\Delta\tau}$ are better approximated with $C_{\sigma} < 8$. All the data fall within the bounds of $4 < C_{\sigma} < 16$ (outer trend lines in Figure 5a).

It is at first surprising that $stdev_{\Delta\tau}$ more strongly affects stress drop than $mean_{\Delta\tau}$. The reason for this is that stress drop is a measure of the average $\Delta\tau_{pot}(x)$ over the ruptured area (Equation 10) not over the entire stress field. Ruptures tend to occur only on sections of $\Delta\tau_{pot}(x)$ with larger-than-average values, so the stress drop is linked to the conditional mean, which scales linearly with the standard deviation.

The relationship from Equation 12 indicates that large variation in $\Delta\tau_{pot}(x)$ causes larger stress drop. Figure 5b shows two examples of $\Delta\tau_{pot}(x)$ with different $stdev_{\Delta\tau}$. Corresponding $G_0(x)$ are shown in Figure 5c, and the two examples produce ruptures of essentially the same length. The $\Delta\sigma^{simp}$ of those two ruptures are shown by the dotted and dashed horizontal lines for the larger and smaller $stdev_{\Delta\tau}$ cases, respectively. The rupture length is the horizontal extent of those lines. Rupture always propagates where $\Delta\tau_{pot}(x)$ is positive on average, and arrests where $\Delta\tau_{pot}(x)$ is negative. Increasing $stdev_{\Delta\tau}$ therefore causes earthquakes to propagate on fault sections with larger average $\Delta\tau_{pot}(x)$ and ultimately arrest at stronger barriers (more negative $\Delta\tau_{pot}(x)$). A more abrupt arrest at a strong barrier produces a higher stress drop.

If large $stdev_{\Delta\tau}$ is associated with geometrically complex fault networks, as suggested in Section 2.1, then the correlation between $\Delta\sigma$ and $stdev_{\Delta\tau}$ found here is consistent with the findings of Lee et al. (2025), who found earthquakes with higher $\Delta\sigma$ were associated with geometrically complex fault networks around the world. The interpretation that average stress drop in a region is controlled by structural features such as fault network complexity is also consistent with the findings of Allmann and Shearer (2007) who found that regions with generally higher- or lower-than-average stress drop remained unchanged by the occurrence of the 2004 Parkfield earthquake.

### 4.2. Mean Stress Affects b-Value

Variables such as $m_{\Delta\tau}$, $mean_{\Delta\tau}$, and $stdev_{\Delta\tau}$ can all affect the distribution of earthquake sizes produced by a stochastic stress field. To illuminate the way that $mean_{\Delta\tau}$ and $m_{\Delta\tau}$ affect b-value, we first consider only cases where 2 MPa $< \Delta\sigma_{\mathbf{M}3} <$ 4 MPa, shown in Figure 6a, consistent with the idea that 3 MPa is the average stress drop observed for a range of earthquake sizes (e.g., Kanamori & Anderson, 1975). Figure 6a shows that increasing $mean_{\Delta\tau}$ causes lower b-value (more large events). This inverse relationship between differential stress and b-value is consistent with laboratory experiments (Bolton et al., 2021; Goebel et al., 2013; Scholz, 1968) and numerical simulations (Ito & Kaneko, 2023). Observational studies also show b-value decreases prior to some

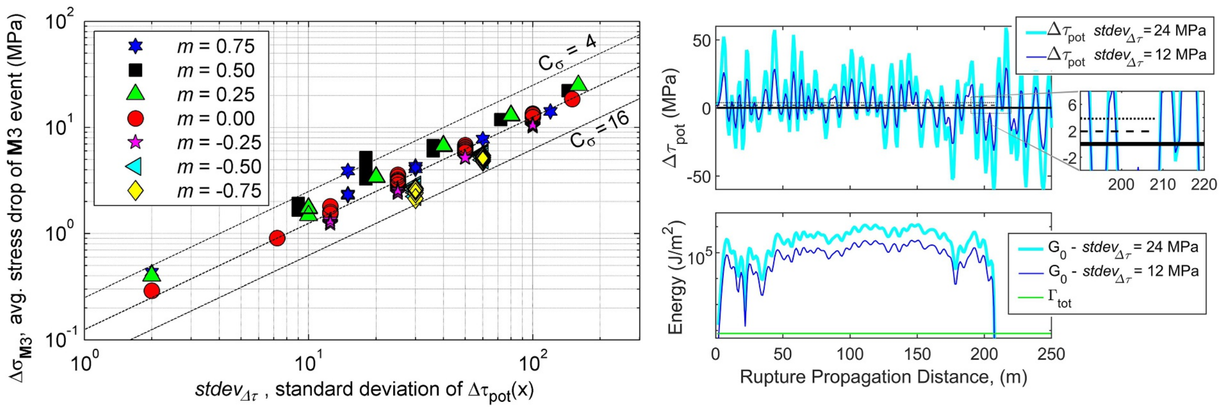

**Figure 5.** Average stress drop of a population, $\Delta\sigma_{\mathbf{M3}}$, is linearly proportional to $stdev_{\Delta\tau}$ of the stress field that created that population, with far smaller dependence on $mean_{\Delta\tau}$ and $m_{\Delta\tau}$. (a) Each marker shows results from a population of simulated earthquakes. All data is presented in Table S1 in Supporting Information S1. The dashed lines are $\Delta\sigma_{\mathbf{M3}} = \mathrm{stdev}_{\Delta\tau}/8$, $\Delta\sigma_{\mathbf{M3}} = \mathrm{stdev}_{\Delta\tau}/4$, and $\Delta\sigma_{\mathbf{M3}} = \mathrm{stdev}_{\Delta\tau}/16$. There is a small dependence on mean stress ($mean_{\Delta\tau}$), shown by $m_{\Delta\tau} = 0.5$ data points with $\mathrm{stdev}_{\Delta\tau} = 18$ MPa and $\Delta\sigma_{\mathbf{M3}} = 5$ MPa that have $mean_{\Delta\tau} = -35$ MPa. (b)–(c) Examples of $\Delta\tau_{\mathrm{pot}}(x)$ (b) and corresponding strain energy release rate $G_0$ (c) showing how increased $\mathrm{stdev}_{\Delta\tau}$ causes a higher stress drop determined as the average $\Delta\tau_{\mathrm{pot}}(x)$ along the rupture length (shown as horizontal dashed and dotted lines for 12 and 24 MPa $\mathrm{stdev}_{\Delta\tau}$ cases, respectively).

earthquakes (Gulia et al., 2016; Nanjo et al., 2012; Tormann et al., 2014) and b-value increases after earthquakes (Gulia & Wiemer, 2019).

To generalize the b-value results and relax the restriction $\Delta\sigma_{\mathbf{M3}} \approx 3$ MPa, we use the parameter *pnr* to characterize the balance between positive and negative $\Delta\tau_{\mathrm{pot}}(x)$. We quantify this positive-negative ratio

$$pnr = -(mean_{\Delta\tau} + stdev_{\Delta\tau})/(mean_{\Delta\tau} - stdev_{\Delta\tau}). \tag{13}$$

Figure 6b shows data from a wide range of stochastic stress fields with a variety of $\Delta\sigma_{\mathbf{M3}}$, and shows that larger *pnr* causes lower b-values. If *pnr* is greater than about 1.18, there will not be enough negative sections to arrest ruptures, and the majority of ruptures will grow very large or fail to arrest entirely. This is consistent with the findings from Ampuero et al. (2006) and Dempsey et al. (2016), who found that decreasing amplitudes of stress heterogeneities (i.e., a smaller $stdev_{\Delta\tau}$ and therefore larger *pnr* given a positive $mean_{\Delta\tau}$) led to a transition from a distribution of earthquake sizes to "characteristic" earthquakes (all earthquakes the same size, low b-values) that

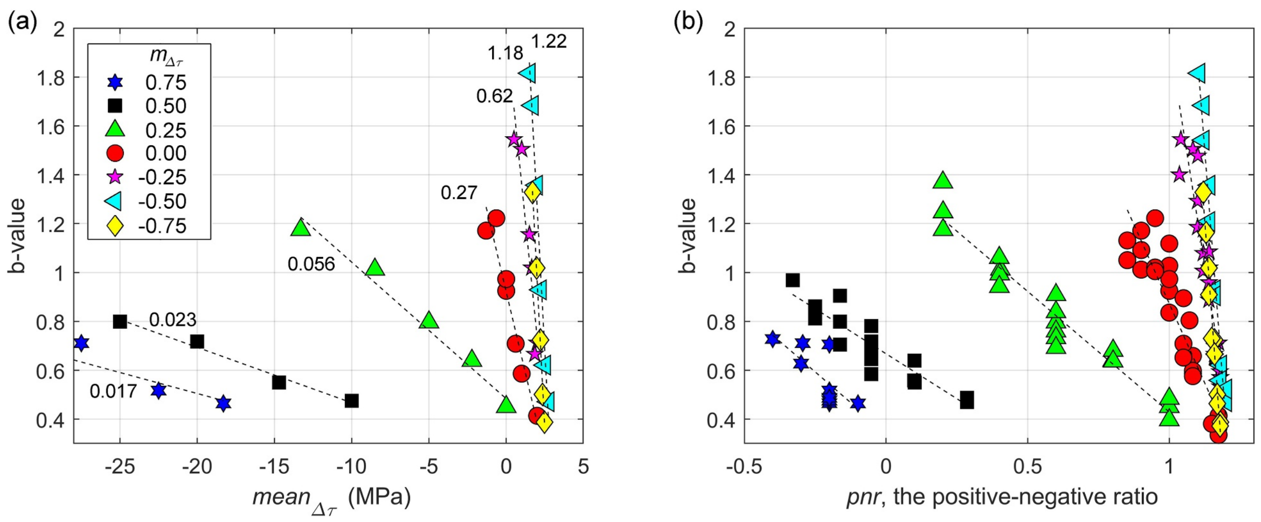

**Figure 6.** Dependence of b-value on (a) mean stress $mean_{\Delta\tau}$ and (b) the positive-negative ratio *pnr*, defined in Equation 13. Large *pnr* values above 1.2 produce mostly large system-spanning events. The data shown in (a) are the subset of those shown in (b) that satisfy 2 MPa $< \Delta\sigma_{\mathbf{M3}} <$ 4 MPa. Stress sensitivity is listed in (a) for each $m_{\Delta\tau}$ in units of b-value/MPa.

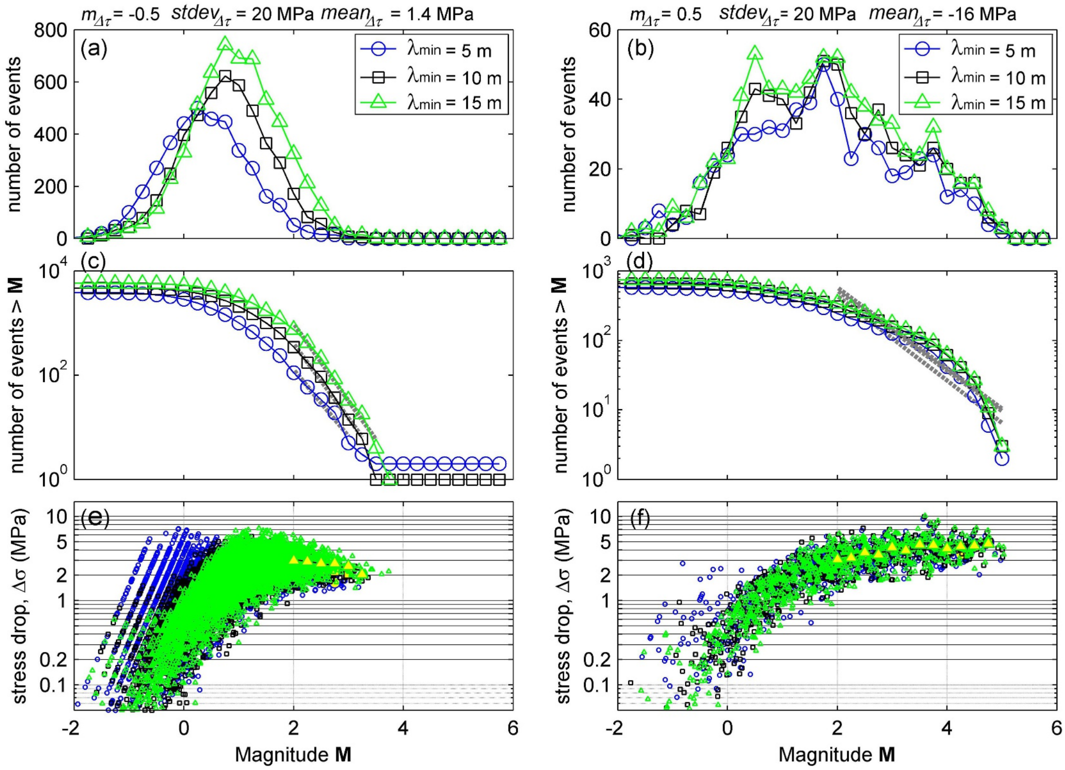


**Figure 7.** The effect of minimum wavelength $\lambda_{\min}$ on earthquake populations is significant for negative $m_{\Delta\tau}$ (left column) and negligible for positive $m_{\Delta\tau}$ (right column). Statistics of the stress fields used to create the populations are shown at the top and in the legend.

were all system-spanning events that never arrested. Our results demonstrate that this transition depends not only on $stdev_{\Delta\tau}$, but also on $mean_{\Delta\tau}$.

### 4.3. $m_{\Delta\tau}$ Affects Stress Sensitivity of b-Value

Figure 6 shows that the relationship between $mean_{\Delta\tau}$ and b-value differs for different values of $m_{\Delta\tau}$. This stress sensitivity is the slope of the dashed lines in Figure 6a, and the various values are listed in units b-value/MPa. This b-value's stress sensitivity may help constrain $m_{\Delta\tau}$. Gulia and Wiemer (2019) reported b-value increases of about 0.2–0.8 for seismicity within 3 km of faults that ruptured in large earthquakes. If it is assumed that average differential stress dropped about 3 MPa in that region, this implies a b-value stress sensitivity of 0.1–0.3 MPa$^{-1}$ $m_{\Delta\tau}$ values of 0.25 and 0 exhibit a sensitive stress sensitivity (0.06 MPa$^{-1}$ and 0.3 MPa$^{-1}$, respectively) that most closely match the Gulia and Wiemer (2019) values.

Stress fields with negative $m_{\Delta\tau}$ exhibit a stronger b-value stress sensitivity (>0.6 MPa$^{-1}$) that is likely inconsistent with observed changes in response to earthquakes. With negative $m_{\Delta\tau}$, a variety of event sizes becomes increasingly difficult to generate because $\Delta\tau_{\text{pot}}(x)$ lacks large-wavelength variation (see Figure 2). If the mean stress is too high, then ruptures fail to arrest, and if the mean stress is too low, then large events are never generated. With negative $m_{\Delta\tau}$, earthquake populations also become strongly dependent on $\lambda_{\min}$, described further in Section 4.4.

On the other hand, $m_{\Delta\tau} > 0.25$ requires an increasingly negative $mean_{\Delta\tau}$ and negative *pnr* to produce earthquake populations with more small events than large ones (i.e., b-values > 0.2). Populations produced with negative *pnr* tend to produce a convexity to the cumulative magnitude frequency distribution (Figure 4b, $m_{\Delta\tau} = 0.5$ case, Figure 7d), as noted by Dempsey et al. (2016), that is inconsistent with natural observations.

### 4.4. The Effects of $\lambda_{min}$

$\lambda_{min}$ generally affects the minimum rupture length and therefore the minimum earthquake size. Figure 7 shows examples of varying $\lambda_{min}$ for cases with $m_{\Delta\tau} = -0.5$ (left side) and $m_{\Delta\tau} = 0.5$ (right side). $\lambda_{min}$ has a strong effect on earthquake populations for negative $m_{\Delta\tau}$ values because $\Delta\tau_{pot}(x)$ becomes dominated by wavelengths near $\lambda_{min}$, but has little effect on earthquake populations when $m_{\Delta\tau} > \sim 0.2$ since $\Delta\tau_{pot}(x)$ is dominated by larger wavelengths, see, for example, Figure 2b.

We chose $M_0^{lowerlimit}$ such that measured parameters of our earthquake populations would not be affected by $\lambda_{min}$ (Section 3.8). We choose $\lambda_{min} = 5\Delta x$, to avoid spatial aliasing and ensure that $\lambda_{min}$ rather than discretization $\Delta x$ affected our results.

### 4.5. Summary of Results With $\Delta\tau_{pot}(x)$ and Constant $\Gamma_{tot}$

With a highly variable $\Delta\tau_{pot}(x)$ and constant $\Gamma_{tot}$ described thus far, (a) stress drop is primarily affected by the variation in $\Delta\tau_{pot}(x)$ (i.e., $stdev_{\Delta\tau}$, Equation 12), (b) b-value is inversely correlated with $mean_{\Delta\tau}$ (i.e., Figure 6a), (c), b-value's stress sensitivity varies systematically with $m_{\Delta\tau}$. The latter may be an opportunity to constrain $m_{\Delta\tau}$ and suggests that $0 \le m_{\Delta\tau} \le 0.25$.

## 5. Effects of Variable $\Gamma_{tot}(x)$

Thus far, we have considered variable $\Delta\tau_{pot}(x)$ while fracture energy $\Gamma_{tot}$ was kept constant at 75 J/m$^2$. Below, we first describe the conditions under which variability in $\Delta\tau_{pot}(x)$ can be replaced by variability in $\Gamma_{tot}(x)$. We then demonstrate the effects of variations in $\Gamma_{tot}$ when $\Delta\tau_{pot}(x)$ is also a highly variable field, as considered in previous sections of this paper.

### 5.1. Variable $\Gamma_{tot}$ $(x)$ Can Replace Variable $\Delta\tau_{pot}(x)$ as Long as $\Gamma_{tot}$ Increases With Rupture Length

When considering the way fracture energy may change along the rupture length $\Gamma_{tot}(x)$, we separate a variable part from a deterministic part, that is,

$$\Gamma_{tot}(x) = \Gamma_{var}(x) + \Gamma_{det}(x). \tag{14}$$

The deterministic part is assumed to have the form

$$\Gamma_{det}(x) = cx^{\beta}, \tag{15}$$

where $c$ is a constant. When $\beta = 0$, then $\Gamma_{tot}$ does not systematically change with rupture propagation distance. When $\beta = 1$ then $\Gamma_{det}$ increases linearly with rupture propagation distance. Many studies have suggested that $\Gamma_{tot}$ might increase with increasing fault slip in an earthquake (e.g., Abercrombie & Rice, 2005; Gabriel et al., 2024; Nielsen et al., 2016), and this might manifest as an increase in $\Gamma_{tot}$ with rupture length (Aochi & Ide, 2004). The scaling implied by Abercrombie and Rice (2005) is $\beta = 1$, $c = 200$ J/m$^2$/m.

$\Gamma_{var}(x)$ is a stochastic field. Similar to $\Delta\tau_{pot}(x)$, it can be defined by its mean ($mean_{\Gamma}$), standard deviation ($stdev_{\Gamma}$), change with wavelength ($m_{\Gamma}$), and minimum wavelength ($\lambda_{min\Gamma}$). We assume $mean_{\Gamma} = 0$, since constant terms are best represented by $\Gamma_{det}(x)$, and we do not consider variations in $\lambda_{min\Gamma}$ since they likely play a minor role.

Figure 8 shows example realizations of $\Gamma_{tot}(x)$ (green and red lines), and how they compare to $G_0$ (black line) derived from Equation 6 and Equation 7 with $\Delta\tau_{pot} = 3$ MPa. When $\Delta\tau_{pot}$ is constant, the slope of $G_0$ on the log-log plot is 1, meaning that $G_0$ increases linearly with rupture propagation distance. The vertical offset of $G_0$ depends on the value of $\Delta\tau_{pot}$. $\Gamma_{tot}(x)$ is expressed according to Equation 14, and the examples shown have $stdev_{\Gamma} = 10$ kJ/m$^2$, $m_{\Gamma}, = 1$, $c = 200$ J/m$^2$/m, and $\beta = 1$ (green) is compared to $\beta = 0.75$ (red).

The examples in Figure 8 show that $\Gamma_{det}(x)$ dominates over $\Gamma_{var}(x)$ when $\Gamma_{det}(x) >> stdev_{\Gamma}$. If $\Gamma_{det}(x) > 10 stdev_{\Gamma}$, then all realizations of $\Gamma_{tot}(x)$ essentially collapse to the same curve. This occurs at $x > 500$ m for $\beta = 1$ cases and at $x > 4{,}000$ m when $\beta = 0.75$. The dominance of $\Gamma_{det}(x)$ at large $x$, means that $\Gamma_{tot}(x)$ and $G_0$ will intersect at one specific rupture length and produce a population of earthquakes that all have similar sizes. Therefore, at large $x$,

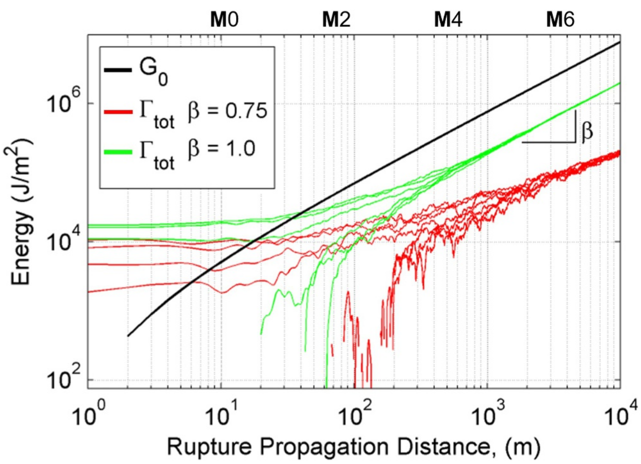


**Figure 8.** The energy balance on a logarithmic scale. Strain energy release rate, $G_0$, increases linearly with rupture length when $\Delta\tau_{pot}$ is constant ($\Delta\tau_{pot} = 3$ MPa is shown). Green and red lines show example populations of $\Gamma_{tot}(x) = cx^{\beta} + \Gamma_{var}(x)$ with differing $\beta$.

the only way for $\Gamma_{tot}(x)$ to remain variable, and therefore produce a variety of events sizes, is if $\Gamma_{var}(x)$ systematically increases with $x$, that is,

$$\Gamma_{tot}(x) = cx^{\beta}\Gamma_{var}(x), \tag{16}$$

as shown in Figure 9c (green trace).

Figure 8 also provides insight into the role of $\beta$. If $\beta = 1$, then $G_0$ and $\Gamma_{det}$ will increase at the same rate and the ratio $G_0/\Gamma_{det}$ will remain approximately constant, so large variations in $\Gamma_{tot}(x)$ will exceed $G_0$ and rupture will arrest. However, if $\beta < 1$, then as the rupture propagates, $G_0$ will become orders of magnitude larger than $\Gamma_{det}$, and even large variations in $\Gamma_{tot}(x)$ will not stop ruptures. This case produces more large earthquakes than small ones. Ruptures will "run away" once high $\Gamma_{tot}$ barriers that are large enough to stop them are rare. On the other hand, if $\beta > 1$, then as the rupture propagates, $\Gamma_{tot}(x)$ will grow larger than $G_0$ near a specific rupture length. This will produce populations of events that are all of a similar size. Only cases with $\beta = 1$ will produce realistic populations of earthquakes with a variety of event sizes.

We explored a variety of scenarios for $\Gamma_{tot}(x)$ but found that those that lack either (a) the increasing variability of $\Gamma_{tot}(x)$ with rupture length, and (b) the linear increase of $\Gamma_{tot}(x)$ with rupture length ($\beta = 1$) never produce realistic populations of earthquakes. This is true even when $\Gamma_{tot}(x)$ varies by many orders of magnitude (such as the magenta line shown in Figure 9c). Figure 9a shows an example of $\Delta\tau_{pot}(x)$ with minimal variability ($mean_{\Delta\tau} = 3$ MPa and $stdev_{\Delta\tau} = 1.5$ MPa). Figure 9c shows its corresponding $G_0$ is similar to the constant $\Delta\tau_{pot}$ case (thicker gray lines). Therefore, the above requirements (increasing $\Gamma_{var}(x)$ and $\beta = 1$) apply to cases with both constant $\Delta\tau_{pot}$, and cases where $stdev_{\Delta\tau}$ is sufficiently small.

An exhaustive search of all scenarios for variable $\Gamma_{tot}$ is outside the scope of the current study. It may be possible that a different form of $\Gamma_{tot}(x)$, such as a Weibull distribution rather than a uniform distribution, could affect our results. We chose to focus on variability in $\Delta\tau_{pot}(x)$. Below we show that with highly variable $\Delta\tau_{pot}(x)$, even strong variability in $\Gamma_{tot}$ has minor effects.

### 5.2. Variable Fracture Energy $\Gamma_{tot}$ When $\Delta\tau_{pot}(x)$ Is Also Highly Variable

Figure 9b shows a case of highly variable $\Delta\tau_{pot}(x)$ with positive and highly negative sections ($mean_{\Delta\tau} = 3$ MPa, $stdev_{\Delta\tau} = 21$ MPa), as considered in the majority of this paper. In this case, $\Gamma_{tot}$ has relatively minor effects on rupture propagation. $\Gamma_{tot} = 75$ J/m$^2$ was chosen for all of the previous simulations and is shown as the thick green line in Figure 9d, however increasing $\Gamma_{tot}$ by one or two orders of magnitude (green dotted lines) does not significantly affect the termination location since rupture termination is controlled by the large variation in $G_0$. To help illustrate this, Figure 10 shows that changing $\Gamma_{tot}$ by many orders of magnitude has a smaller effect on b-values than a 1 MPa change in $mean_{\Delta\tau}$. Thus, when $\Delta\tau_{pot}(x)$ is already highly variable, adding variability to $\Gamma_{tot}$ has a relatively minor effect. However, if $\Gamma_{tot}$ is increased above a certain threshold (about 10,000 J/m$^2$ for the conditions studied here), few earthquakes can propagate at all, so the b-value becomes strongly affected.

## 6. Discussion

### 6.1. Realistic Earthquake Populations Require Highly Variable and Highly Negative $\Delta\tau_{pot}(x)$

A key insight provided by this study is that fault systems that produce a variety of event sizes require $\Delta\tau_{pot}(x)$ to be highly variable. The variability in $\Delta\tau_{pot}(x)$ must far exceed the mean, meaning that $\Delta\tau_{pot}(x)$ must include both positive and significantly negative values. As long as $m_{\Delta\tau}$ is less than approximately 0.25, as suggested in Section 4.4, this variability is strong at short length scales—10s of meters (i.e., the size of a **M** 1 earthquake) but likely even smaller. The rapid oscillation between highly positive $\Delta\tau_{pot}(x)$ and highly negative $\Delta\tau_{pot}(x)$ dictates that as an earthquake rupture propagates, it alternates between periods of rapid rupture acceleration and deceleration. This likely produces "subevents" within an earthquake rupture (i.e., Danré et al., 2019; Houston, 2001; Yoshida & Kanamori, 2023) as well as seismic radiation at a broad range of frequencies (e.g., Dunham

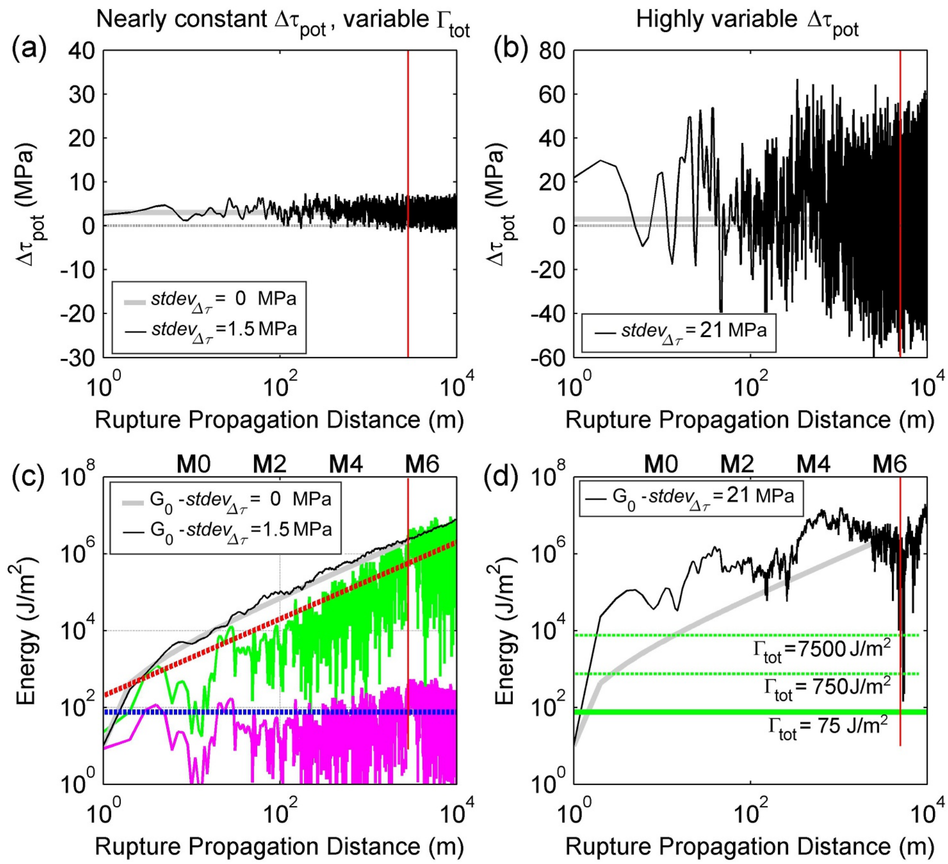


**Figure 9.** Examples of $\Delta\tau_{pot}(x)$ and corresponding $G_0$ similar to Figure 3 except on a logarithmic distance scale. (a)–(b) Examples of $\Delta\tau_{pot}(x)$ with $m_{\Delta\tau} = 0.25$, $mean_{\Delta\tau} = 3$ MPa, and (a) $stdev_{\Delta\tau} = 1.5$ MPa (b) $stdev_{\Delta\tau} = 21$ MPa. The thick gray line shows $\Delta\tau_{pot}(x) = 3$ MPa. (c)–(d) $G_0(x)$ corresponding to $\Delta\tau_{pot}(x)$ shown in a-b, respectively. (c) Relatively modest variability in $\Delta\tau_{pot}(x)$ (i.e., $stdev_{\Delta\tau}/mean_{\Delta\tau} = 0.5$) produces $G_0$ (black line) that is not significantly different from constant $\Delta\tau_{pot} = 3$ MPa (thick gray lines). In this case, $\Gamma_{tot}(x)$ must systematically increase with rupture length (green lines) since even highly variable $\Gamma_{tot}(x)$ that lacks this systematic scaling (magenta lines) cannot produce realistic populations of ruptures. (d) Highly variable $\Delta\tau_{pot}(x)$ (i.e. $stdev_{\Delta\tau}/mean_{\Delta\tau} = 7$) produces $G_0$ that differs significantly from the constant $\Delta\tau_{pot} = 3$ MPa case (gray lines) both due to high $G_0$ values at small propagation distances and occasional reductions in $G_0$ that can arrest ruptures at any distance, with little sensitivity to $\Gamma_{tot}$.

et al., 2011). Future work might link the stochastic stress field to the $\omega^{-2}$ falloff of high-frequency radiation observed for most earthquakes, but this is outside the scope of the current study.

An equally important requirement to produce realistic earthquake populations with a variety of event sizes is a seismogenic fault domain $L$ that is large relative to the nucleation length scale $L_c$. Earthquake cycle simulations show that a variety of event sizes emerge from large $L/L_c$ (e.g., Barbot, 2019; Cattania, 2019; Perry et al., 2020), but combining large $L/L_c$ (e.g., >500) with sophisticated modeling remains computationally prohibitive, even on a 1D fault. In contrast, the simplified fracture-mechanics-based modeling approach employed in this study allows $L/L_c \approx 10{,}000$, since $L_c < \Delta x$ (Section 3.2) and $L = n\Delta x$ with $n = 10{,}000$ (Section 3.8).

### 6.2. Connection Between $m_{\Delta\tau}$ and Measured Fault Roughness

The topography of fault surfaces $u(x)$ has been measured to have a roughness exponent $m_u \approx 1.1$ ($H \approx 0.6$) (Brodsky et al., 2016). Equations 1 and 2 suggest that $\Delta\tau_{pot}(x)$ should be one or maybe two derivatives of the fault roughness, which would subtract 1 or perhaps 2 from the value of $m_u$. Thus, we would expect $m_{\Delta\tau} \approx 0.1$, though it might be as low as −0.9.

Because of the ambiguity in the quantitative value of b-value in our model and how it might change from 1D ruptures to 2D ruptures, it is difficult to precisely constrain $m_{\Delta\tau}$ with our method; however, we argue that fields

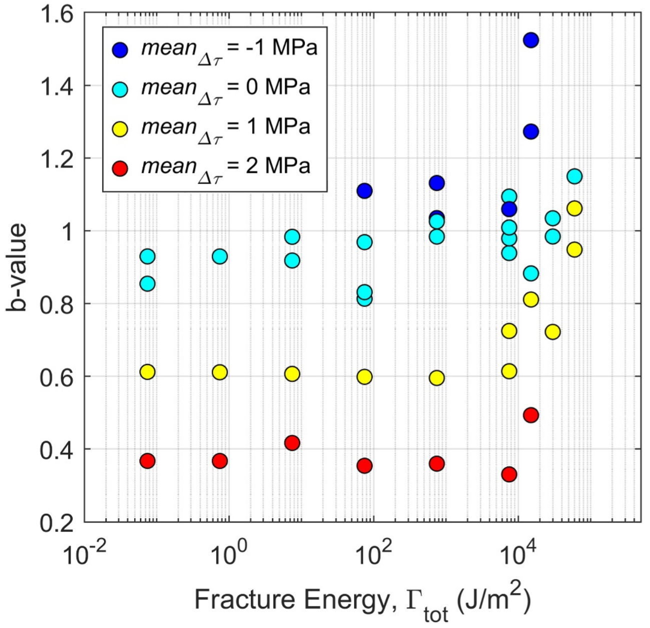


**Figure 10.** In cases where $\Delta\tau_{pot}(x)$ is highly variable, b-value is insensitive to $\Gamma_{tot}$ for $\Gamma_{tot} \leq 10{,}000$ J/m$^2$. Each symbol is a population of earthquakes similar to Figures 5 and 6. For all populations, $stdev_{\Delta\tau} = 24$ MPa, $m_{\Delta\tau} = 0$, $\Gamma_{tot}$ is constant at the value indicated on the $x$ axis. b-value is far more sensitive to $mean_{\Delta\tau}$, indicated by different symbol colors.

with $m_{\Delta\tau} < 0$ exhibit a b-value stress sensitivity that is likely too strong, and fields with $m_{\Delta\tau} > 0.25$ produce convex magnitude frequency distributions and require a $mean_{\Delta\tau}$ that is likely too low, as discussed further in Section 4.4. Thus, our preferred models have $0 \leq m_{\Delta\tau} \leq 0.25$, and are therefore roughly consistent with the above interpretation of stresses resulting from measured fault roughness.

### 6.3. Earthquake Initiation on Rough Faults

A key assumption in this work is that earthquakes initiate at random locations and at very small length scales, not at specific features of $\Delta\tau_{pot}(x)$, and not according to a nucleation process. But is this realistic?

The way in which earthquakes initiate on rough faults is poorly understood. Conceptual models of earthquake nucleation and a critical nucleation length, $L_c$, are based on laboratory experiments (e.g., McLaskey, 2019; Ohnaka & Kuwahara, 1990) and theories (e.g., Dieterich, 1992; Rubin & Ampuero, 2005) that employ flat faults and neglect realistic fault architecture. Some studies showed how heterogeneous fault properties can significantly modify this "flat-fault" nucleation process (Cattania & Segall, 2021; Tal et al., 2018), but this is an active area of research.

Evidence from nature overwhelmingly suggests that earthquakes initiate and become fully dynamic at a small length scale, similar to the abrupt initiation assumption employed here. First, the existence of small earthquakes ~ **M** −1.5, suggests $L_c < 1$ m (Wu & McLaskey, 2022) at seismogenic depths. In fact, no lower magnitude limit has been robustly observed, at least down to **M** −4 (Boettcher et al., 2009; Kwiatek et al., 2011). A small nucleation length is also supported by evidence of universal earthquake rupture growth (e.g., Meier et al., 2017; Uchide & Ide, 2010) and small and large earthquakes with identical initial waveforms (e.g., Ide, 2019). There are certainly tectonic environments where aseismic slip and earthquakes coexist, and aseismic slip prior to some subduction zone earthquakes might be interpreted as related to "flat-fault" earthquake nucleation with $L_c$ on the order of 10s of kms (e.g., Kato et al., 2012). But the vast majority of earthquakes, particularly those on less-mature crustal faults, are not preceded by detectable aseismic slip (e.g., Roeloffs, 2006). Some studies also showed that "flat-fault" earthquake nucleation can be circumvented in favor of an abrupt nucleation at a small length scale (McLaskey & Lockner, 2014; Noda et al., 2013), even on faults with only mild heterogeneity, in a mechanism termed "rate dependent cascade up" (McLaskey, 2019).

Where do earthquakes initiate? Coulomb friction suggests that slip initiates at a maximum in $\tau_0(x)/\sigma_N(x)$. If effective normal stress $\sigma_N$ was constant, then this would suggest that earthquakes initiate at maxima of $\Delta\tau_{pot}(x)$, which is quite different from our assumption of random initiation location. However, there is strong evidence to suggest that $\sigma_N(x)$ is highly variable on rough faults, and that low values of $\sigma_N(x)$ are a more potent way to maximize $\tau_0(x)/\sigma_N(x)$ and initiate slip. Laboratory experiments (Ben-David et al., 2010) and numerical simulations (e.g., Cattania & Segall, 2021) both indicate that slip tends to initiate at minima in $\sigma_N(x)$. High pore fluid-pressures also reduce $\sigma_N$ and can be an effective mechanism to initiate fault slip (e.g., Cebry et al., 2022; Guglielmi et al., 2015; Raleigh et al., 1976). Variable $\sigma_N(x)$ due to slip of rough faults is likely proportional to the curvature of fault roughness (Equation 2), the second spatial derivative. Thus, if $m_u \approx 1.1$, as observed for exhumed faults (Brodsky et al., 2016), then the $m$ value of $\sigma_N(x)$ would be $1.1–2 = -0.9$. (For a visual example of such a $\sigma_N(x)$, consider the $m_{\Delta\tau} = -0.5$ case in Figure 2a.) This means that slip on naturally rough faults produce minima in $\sigma_N(x)$ at the shortest spatial scales resolvable. In other words, slip can initiate nearly anywhere.

If stresses are indeed highly variable due to complex fault architecture, as suggested by this study, then random initiation at unresolvably small length scales may be a perfectly adequate first-order modeling choice, and adherence to a "flat-fault" nucleation criterion will only bias results in a way that is inconsistent with natural observations.

### 6.4. Variable and Negative $\Delta\tau_{pot}$ Produced by Slip on Rough Faults and Complex Fault Architecture

How can a highly variable and extremely negative $\Delta\tau_{pot}$ come to exist? Slip on rough faults has been shown to produce a highly heterogeneous shear stress distribution (Cattania & Segall, 2021; Dieterich & Smith, 2009; Dunham et al., 2011; Fang & Dunham, 2013; Romanet et al., 2020, 2024; Wise & Tal, 2024). e.g., Dieterich and Smith (2009) showed that local deviations from planarity that are 1% of the wavelength (i.e. 100 mm deviations over a spatial scale of 10 m) would generate shear stress changes on the order of 300 MPa if the wall rocks remained elastic. Brodsky et al. (2016) compiled measurements from exhumed fault surfaces and found deviations from planarity at 1–10 m length scales on the order of 0.1% (10 mm deviations over 10 m scale), which would suggest 30 MPa stress changes. As pointed out previously (e.g., Dunham et al., 2011), those roughness measurements are from single faults, and the combination of structures that accommodate displacement in an earthquake might be more accurately described as a rougher surface. Based on this, we suggest that slip on rough faults or complex fault networks can likely produce variations in shear stress on the order of 100 MPa. The above studies assume elastic material properties, and large increases in stress will likely be limited by brittle fracture and other material limits. However, for large decreases in shear stress that reduce $\tau_0$ far below $\tau_r$ and produce negative $\Delta\tau_{pot}$ those material limits are not as strict. Slip of rough faults also produces heterogeneous $\sigma_N(x)$, which suggests heterogeneous $\tau_r(x)$. This might be another mechanism for variable and negative $\Delta\tau_{pot}(x)$. Overall, slip within fault zones with complex architecture may be a likely mechanism for the highly variable and extremely negative values of $\Delta\tau_{pot}$ that appear to be necessary to produce populations of earthquakes with a variety of sizes.

Heterogeneous stresses from slip on rough faults or complex fault zones might develop coseismically from heterogeneous slip in earthquakes; however, those stresses could possibly be countered by inelastic and thermally activated processes in the earth that act to smooth the stress distribution through a mechanism that might be modeled as viscoelastic relaxation.

It may also be possible that heterogeneous stresses develop interseismically and are associated with heterogeneous afterslip (e.g., Floyd et al., 2016) or other slow processes. For example, Sirorattanakul et al. (2025) recently measured slowly accumulating slip on laboratory samples held under constant load in essentially stationary contact over many hours, in a process related to fault healing or "aging," a mechanism that underpins the rate- and state-dependent friction equations (e.g., Dieterich, 1979; Ruina, 1983). Figure 11a shows the spatial distribution of slip $\delta(x)$ measured by Sirorattanakul et al. (2025) after 2 hr, 20 hr, and 200 hr on a laboratory fault made from the interface between roughened polymer blocks and held with a constant 4 MPa shear stress. The average amount of slip increases approximately linearly in log time, as shown in Figure 11b, but the standard deviation of the slip distribution also increases over time (Figure 11c). Heterogeneous slip $\delta(x)$ causes heterogeneous stress changes, so the increase in the standard deviation indicates that stresses became more heterogeneous as the sample "aged" in essentially stationary contact. (Note that the authors ruled out bulk viscoelastic deformation of the polymer as a mechanism for the observed slip and they also found similar results when a 2 mm thick layer of quartz gouge was placed on the interface between the polymer blocks.)

Shear stress changes $\Delta\tau(x)$ are proportional to the gradient of slip (e.g., Bilby & Eshelby, 1968), and if it is assumed that shear modulus $\mu = 1.7$ GPa, then the measured slip gradient $d(\delta)/dx = 0.002$ (i.e., 2 μm of slip over a length scale of 1 mm) and application of the back-of-the-envelope calculation $\Delta\tau \approx \mu\, d(\delta)/dx$ suggests stress changes on the order of $\pm 3.4$ MPa. This indicates that locally variable stress changes associated with healing and aging of a (laboratory) fault can be of a similar magnitude to the average shear stress carried by that fault. If similar healing and aging mechanisms occur on natural fault zones, they would appear to provide a mechanism for the heterogeneous stresses required to support the conclusions of this study.

#### 6.4.1. Other Mechanisms for Negative $\Delta\tau_{pot}$

Other candidate mechanisms for negative $\Delta\tau_{pot}$ exist. For example, fault sections with velocity strengthening (VS) frictional behavior cause faults to possess a sliding strength that exceeds the initial stress level, and this produces negative $\Delta\tau_{pot}$. VS behavior is usually associated with specific fault zone minerals such as phyllosilicates (e.g., Ikari et al., 2011), so this mechanism suggests a more permanent character to the negative $\Delta\tau_{pot}(x)$ sections that may not be easily reconfigured by fault slip. While VS mechanisms may be dominant in subduction zones or other faults that host persistently repeating earthquakes, they may not be as universal of a feature as fault roughness/architecture.

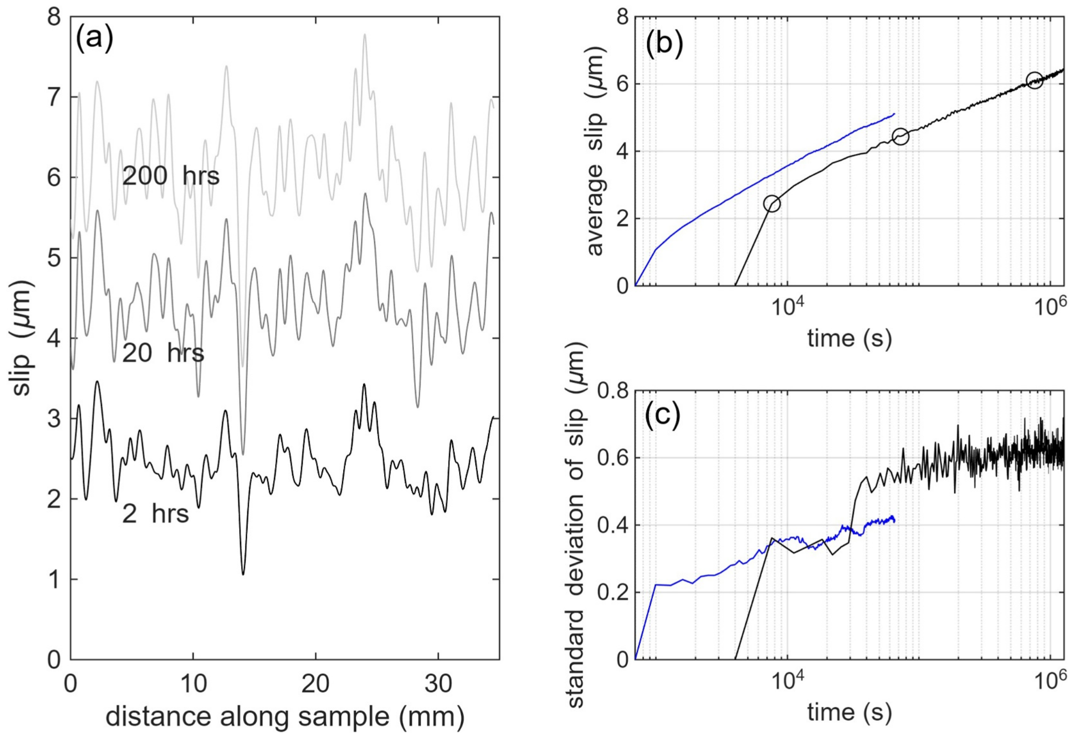


**Figure 11.** Variable slip during fault aging as a mechanism for heterogeneous stresses. (a) Three examples of the spatial distribution of slip $\delta(x)$ measured by Sirorattanakul et al. (2025) after 2 hr, 20 hr, and 200 hr on a polymer fault held in essentially stationary contact under 4 MPa sample average shear stress and 8 MPa sample-average normal stress. (b) The evolution of the average of $\delta(x)$ showing approximately linear increases in slip over log time. The circles show the times of the measurements shown in (a). (c) The evolution of the standard deviation of $\delta(x)$. Blue lines in (b) and (c) show a second experiment with similar results conducted with a shorter temporal sampling interval and shorter overall duration.

Negative $\Delta\tau_{\mathrm{pot}}(x)$ can also be created by stress overshoot, a condition observed even on planar faults; however, overshoot found in numerical simulations (i.e., Madariaga, 1976; Ke et al., 2022) is typically limited to less than 20% of $\Delta\sigma$, making it an unlikely candidate for the more extreme values required by this study.

### 6.5. Stress Drop, Strength Excess, and the Strength of the Crust

Earthquake stress drop $\Delta\sigma$ has been found to be ~1–10 MPa, independent of magnitude and largely independent of depth (Allmann & Shearer, 2009; Denolle & Shearer, 2016; Kanamori & Anderson, 1975). Magnitude-independent stress drop occurs naturally with our preferred models. Further, effective normal stress, $\sigma_N$, has only minor effects on our model. It affects $\Gamma_{\mathrm{tot}}$ (Section 3.5, Equation 8), but Section 5.2 showed that our model results were insensitive to orders of magnitude variations in $\Gamma_{\mathrm{tot}}$ (and thus similar variations in $\sigma_N$). $\sigma_N$ also plays a role in the earthquake initiation criterion, but arguments in Section 6.3 suggest that for earthquakes that occur in naturally rough/complex fault zones, it is variability in $\sigma_N(x)$ that likely controls earthquake initiation, and that the average $\sigma_N$ plays a negligible role. Since our model results show a lack of dependence on $\sigma_N$, they are roughly consistent with the observation that $\Delta\sigma$ is largely independent of depth. The above inferences also indicate that the parameter $(\tau_p–\tau_0)$ referred to as "strength excess" or "stress to failure" plays a minimal role and is far subordinate to $\Delta\tau_{\mathrm{pot}} = \tau_0–\tau_r$.

The connection between $\Delta\sigma$ and $stdev_{\Delta\tau}$ highlighted in this study (Section 4.1) suggests a link between the observed value of earthquake stress drops (1–10 MPa) and the strength of the brittle crust. If we impose the constraint $\Delta\sigma \approx \Delta\sigma_{\mathbf{M3}} = 1–10$ MPa and assume $C_\sigma = 8$, then Equation 12 suggests $stdev_{\Delta\tau} = 8–80$ MPa. That stress-drop-constrained characteristic of $\Delta\tau_{\mathrm{pot}}(x)$ is broadly consistent with the bounds on $\Delta\tau_{\mathrm{pot}}$ placed by the strength of the brittle crust. For example, $\Delta\tau_{\mathrm{pot}}$ must be less than the peak shear strength $\tau_p$ because $\Delta\tau_{\mathrm{pot}} = \tau_0–\tau_r$ and $\tau_r \geq$ zero, and $\tau_0$ cannot exceed $\tau_p$, otherwise the fault would start to slip and reduce $\tau_0$. Assuming that at seismogenic depths of 5–15 km, the effective normal stress $\sigma_N = 50–150$ MPa, then Byerlee (1978) friction

($\tau_p \approx 0.7\sigma_N$) puts an upper bound on $\Delta\tau_{\text{pot}} = 35$–$105$ MPa. Thus the maximum possible $\Delta\tau_{\text{pot}}$ is somewhat larger but of the same order of magnitude as the $stdev_{\Delta\tau}$ required to match $\Delta\sigma = 1$–$10$ MPa. Put differently, Equation 12 shows that $\Delta\sigma$ is roughly an order of magnitude smaller than the variability of $\Delta\tau_{\text{pot}}$, so the maximum variability of $\Delta\tau_{\text{pot}}$ that is permissible based on the Byerlee (1978) crustal strength (i.e., 10–100 MPa), produces $\Delta\sigma \approx 1$–$10$ MPa, as observed globally. This highly variable stress model proposed here suggests that earthquake stress drop values reflect the limits placed by the strength of rocks. (Note that the above arguments only assume Byerlee friction for peak strength $\tau_p$ and certainly allow for dynamic weakening, i.e. $\tau_r \approx 0$.)

### 6.6. Connection to Current Earthquake Models

The highly variable and highly negative $\Delta\tau_{\text{pot}}(x)$ suggested by this study differs significantly from the way that stress and strength are commonly viewed and modeled today. For example, a positive and constant $\Delta\tau_{\text{pot}}$ is assumed in nearly all of the seminal studies that shaped our basic understanding of earthquake mechanics (e.g., Andrews, 1976; Brune, 1970; Madariaga, 1976). Even when heterogeneity has been considered, it is either not as strong as this study suggests (e.g., Andrews, 1980) or negative values of $\Delta\tau_{\text{pot}}$ are not considered (i.e., Renou et al., 2022; Venegas-Aravena et al., 2024). A common way to formulate shear stress in dynamic rupture models is to project a smooth regional stress orientation onto an assumed fault geometry that is based on a depth extension of mapped surface faults (e.g., Ando & Kaneko, 2018; Ulrich et al., 2019). This practice results in mild stress heterogeneity because it lacks stress variation due to slip of rough faults and complex fault zones (Section 6.4). For studies that directly model slip on rough faults (e.g., Dunham et al., 2011; Heimisson, 2020; Shi & Day, 2013; Tal & Hager, 2018), the ranges of $\Delta\tau_{\text{pot}}(x)$ explored are dictated by assumptions about fault friction, initial stresses, and stress relaxation mechanisms. High computational cost also limits the parameter space considered with rough-fault-slip simulations; for example, only self-similar roughness ($m_u = 1.5$) has been studied. Nevertheless, it would be interesting to estimate the $\Delta\tau_{\text{pot}}(x)$ that is produced by those models and compare it to the form suggested by this study.

Earthquake studies often suggest that small earthquakes arise from small faults or small seismogenic asperities or small wavelength variations of $\Delta\tau_{\text{pot}}(x)$, and large earthquakes are produced by larger faults or large seismogenic asperities or large wavelength variations in $\Delta\tau_{\text{pot}}(x)$ (e.g., Hanks, 1979; Ohnaka, 2003). However, the short wavelength variations and negative values of $\Delta\tau_{\text{pot}}(x)$ prevalent in the preferred models of this study ($m_{\Delta\tau} \approx 0$) suggest that nearly all earthquakes—even small ones—traverse multiple asperities and barriers (positive and negative sections of $\Delta\tau_{\text{pot}}$). On a large scale, this type of behavior may be akin to a rupture jumping from one fault to another, as observed for many large strike-slip earthquake (Landers 1992; Kaikoura 2016; Turkey, 2023), but because variability in $\Delta\tau_{\text{pot}}(x)$ is likely related to fault roughness that has been shown to affect multiple scales, we expect a similar "rupture jumping" behavior to occur at nearly all scales.

Stresses that are below the sliding strength of faults are not common in standard earthquake rupture simulations (e.g., Gabriel et al., 2024; Harris et al., 2021; Tinti et al., 2021). In most models, earthquakes only stop because the fault comes to an end (i.e., a barrier of infinite strength or infinitely negative $\Delta\tau_{\text{pot}}$) or because they propagate into a velocity-strengthening fault section (also strongly negative $\Delta\tau_{\text{pot}}$) (e.g., Perry et al., 2020). This study suggests that earthquake ruptures must traverse fault sections that alternate between negative and positive values of $\Delta\tau_{\text{pot}}$. Fault sections with negative $\Delta\tau_{\text{pot}}(x)$ sap energy from the rupture, slow it down, and threaten to arrest it. Therefore, models without negative $\Delta\tau_{\text{pot}}(x)$ require a very large fracture energy to prevent sustained supershear rupture propagation. Yet, those conditions—large fracture energy and nearly constant $\Delta\tau_{\text{pot}}(x)$—do not allow for populations of both large and small earthquakes. Those characteristics necessitate a fracture energy that systematically scales with rupture length.

Some qualities of seismogenic faults suggested by this study might be directly implemented as modifications to current modeling approaches. For example, sections of negative $\Delta\tau_{\text{pot}}(x)$ might be introduced to dynamic rupture models. Variability of $\Delta\tau_{\text{pot}}(x)$ on very small length scales, however, might not be achievable or computationally tractable, so the effects of highly variable $\Delta\tau_{\text{pot}}(x)$ at smaller length scales might be modeled with a physically realistic simplification that accounts for the systematic differences between energy release rates shown in Figures 9c and 9d.

## 7. Conclusions, Limitations, and Future Work

The stochastic models in this study are highly simplified and 1D; however, their good agreement with multiple characteristics of natural earthquake populations suggests that they capture much of the key physics of dynamic rupture propagation and arrest, and warrant further studies. For example, the highly variable stress fields required to produce earthquake populations with a variety of rupture sizes also produce earthquake ruptures that nearly arrest and rapidly reaccelerate. This is consistent with observations of earthquake source time functions with multiple sub-events (Section 6.1) and provides a likely mechanism for high-frequency ground motion that is lacking in many current dynamic rupture models that employ smoother stress fields. We also observe that b-value decreases with increasing average shear stress, consistent with lab results and observations from natural earthquakes (Section 4.3). Surprisingly, this study indicates that stress drop $\Delta\sigma$ primarily increases with increasing $stdev_{\Delta\tau}$ rather than $mean_{\Delta\tau}$. Further, when we impose the constraint $\Delta\sigma = 1\text{–}10$ MPa, to match global stress drop observations, the resulting constraints on $\Delta\tau_{\text{pot}}$ are broadly consistent with Byerlee (1978) friction and the strength of rocks at seismogenic conditions (Section 6.5).

A limitation of this study is that the model utilizes only the energy balance at the rupture front to dictate earthquake size. The effects of energy release and additional dissipation far behind the primary rupture front may generate multiple rupture fronts and may influence the mechanics of earthquakes in ways that are not captured in the current model formulation. Similarly, the formulation of strain energy release rate (Equations 6 and 7) assumes a crack-like rupture and would need to be modified for a self-healing slip pulse. Implicit in this formulation is an assumption that sliding strength $\tau_r$ is equal to the final strength (i.e., no undershoot or overshoot) and therefore earthquake stress drop $\Delta\sigma$ can be calculated from $\Delta\tau_{\text{pot}}$ (Equation 10). Future work might explore 2-dimensional rupture propagation in the variable stress field $\Delta\tau_{\text{pot}}$(x,y), expanding on Ripperger et al. (2007). This will allow the study of how ruptures propagate around barriers in 2D. With 2D rupture, parameters such as stress drop and b-value can be more precisely linked to field constraints.

Another goal of future work might be to develop a framework where both $\Gamma_{\text{tot}}(x)$ and $\Delta\tau_{\text{pot}}(x)$ are inherited from fault topography and slip-induced stress changes from previous events. Such a framework might be an opportunity to address non-random phase. The self-affine realizations of $\Delta\tau_{\text{pot}}(x)$ we utilize in this study have random phase, a characteristic that may not be shared by real fault topography and the stress fields that they produce. However, accurate characterization of the heterogeneous stress changes associated with slip on rough/complex fault zones requires a balance between elastic and inelastic processes and assumptions about failure criteria and time-dependent deformation mechanisms, all of which are avoided in the current approach.

This study did not model earthquake sequences, where $\Delta\tau_{\text{pot}}(x)$ is conditioned by previous ruptures (e.g., Oral et al., 2022). Each rupture in the populations studied here experienced a "fresh" distribution of $\Delta\tau_{\text{pot}}(x)$ defined by the four statistical parameters. As pointed out by Andrews (1980), tectonic loading and standard crack models (i.e., Burridge & Halliday, 1971; Ke et al., 2021) tend to smooth the stress field. If the statistics of $\Delta\tau_{\text{pot}}(x)$ are largely maintained over multiple earthquake ruptures, then $\Delta\tau_{\text{pot}}(x)$ must be re-roughened, perhaps by fracture misalignment, heterogeneous slip (e.g., Manighetti et al., 2001), or postseismic and interseismic healing and aging processes that might occur on both large and small length scales (e.g., Floyd et al., 2016; Sirorattanakul et al., 2025).

## Conflict of Interest

The authors declare no conflicts of interest relevant to this study.

## Availability Statement

MATLAB scripts for how to generate the stochastic stress fields and corresponding populations of earthquakes are freely available at McLaskey et al. (2026). The data for Figure 11 can be found in Sirorattanakul et al. (2025).

**Acknowledgments**
We thank Ahmed Elbana and an anonymous reviewer for helpful comments on the paper. G.C.M. acknowledges the sabbatical program at Cornell University that allowed time to evaluate the important problems, many conversations with Camilla Cattania, Joseph Van Linn, and Dibya Basu, helpful tips from David Dempsey, comments on the manuscript from Emily Brodsky, a long-ago conversation with Jessica Hawthorne who suggested Ripperger et al. (2007), and suggestions by Bill Ellsworth over the years such as, "maybe earthquake nucleation is not what matters" and "check out Dempsey and Suckale." G.C.M. and C.-Y. K. thank the NTU-Cornell Global Strategic Collaboration award for support. G.C.M. gratefully acknowledges that this work was supported, in part, by National Science Foundation Grant EAR-2240375.

## References

Abercrombie, R. E., & Rice, J. R. (2005). Can observations of earthquake scaling constrain slip weakening? *Geophysical Journal International*, *162*(2), 406–424. https://doi.org/10.1111/j.1365-246x.2005.02579.x

Albertini, G., Simon, K., Grigoriu, M. D., & Kammer, D. S. (2021). Stochastic properties of static friction. *Journal of the Mechanics and Physics of Solids*, *147*, 104242. https://doi.org/10.1016/j.jmps.2020.104242

Allmann, B., & Shearer, P. (2007). Spatial and temporal stress drop variations in small earthquakes near Parkfield, California. *Journal of Geophysical Research*, *112*(B4), B04305. https://doi.org/10.1029/2006jb004395

Allmann, B. P., & Shearer, P. M. (2009). Global variations of stress drop for moderate to large earthquakes. *Journal of Geophysical Research*, *114*(B1), B01310. https://doi.org/10.1029/2008jb005821

Ampuero, J.-P., Ripperger, J., & Mai, P. M. (2006). Properties of dynamic earthquake ruptures with heterogeneous stress drop. In R. Abercrombie (Ed.), *Radiated energy and the physics of earthquake faulting, geophys. Monogr. Ser*. (Vol. 70, pp. 3–13). AGU.

Ando, R., & Kaneko, Y. (2018). Dynamic rupture simulation reproduces spontaneous multifault rupture and arrest during the 2016 Mw 7.9 Kaikoura earthquake. *Geophysical Research Letters*, *45*(23), 12–875. https://doi.org/10.1029/2018gl080550

Andrews, D. J. (1976). Rupture velocity of plane strain shear cracks. *Journal of Geophysical Research*, *81*(32), 5679–5687. https://doi.org/10.1029/jb081i032p05679

Andrews, D. J. (1980). A stochastic fault model. *Journal of Geophysical Research*.

Aochi, H., & Ide, S. (2004). Numerical study on multi-scaling earthquake rupture. *Geophysical Research Letters*, *31*(2), L02606. https://doi.org/10.1029/2003gl018708

Barbot, S. (2019). Slow-slip, slow earthquakes, period-two cycles, full and partial ruptures, and deterministic chaos in a single asperity fault. *Tectonophysics*, *768*, 228171. https://doi.org/10.1016/j.tecto.2019.228171

Barton, C., & Zoback, M. D. (1994). Stress perturbations associated with active faults penetrated by boreholes: Possible evidence for near-complete stress drop and a new technique for stress magnitude measurement. *Journal of Geophysical Research*, *99*(B5), 9373–9390. https://doi.org/10.1029/93jb03359

Bayart, E., Svetlizky, I., & Fineberg, J. (2016). Fracture mechanics determine the lengths of interface ruptures that mediate frictional motion. *Nature Physics*, *12*(2), 166–170. https://doi.org/10.1038/nphys3539

Bayart, E., Svetlizky, I., & Fineberg, J. (2018). Rupture dynamics of heterogeneous frictional interfaces. *Journal of Geophysical Research: Solid Earth*, *123*(5), 3828–3848. https://doi.org/10.1002/2018jb015509

Beeler, N. M. (2023). On the scale-dependence of fault surface roughness. *Journal of Geophysical Research: Solid Earth*, *128*(2), e2022JB024856. https://doi.org/10.1029/2022jb024856

Ben-David, O., Cohen, G., & Fineberg, J. (2010). The dynamics of the onset of frictional slip. *Science*, *330*(6001), 211–214. https://doi.org/10.1126/science.1194777

Bilby, B. A., & Eshelby, J. D. (1968). Dislocations and the theory of fracture. In H. Liebowitz (Ed.), *Fracture, an advanced treatise* (Vol. I, pp. 99–182). Academic. chap. 2.

Boettcher, M. S., McGarr, A., & Johnston, M. (2009). Extension of Gutenberg-Richter distribution to Mw–1.3, no lower limit in sight. *Geophysical Research Letters*, *36*(10), L10307. https://doi.org/10.1029/2009gl038080

Bolton, D. C., Shreedharan, S., Rivière, J., & Marone, C. (2021). Frequency-magnitude statistics of laboratory foreshocks vary with shear velocity, fault slip rate, and shear stress. *Journal of Geophysical Research: Solid Earth*, *126*(11), e2021JB022175. https://doi.org/10.1029/2021jb022175

Brodsky, E. E., Kirkpatrick, J. D., & Candela, T. (2016). Constraints from fault roughness on the scale-dependent strength of rocks. *Geology*, *44*(1), 19–22. https://doi.org/10.1130/g37206.1

Brodsky, E. E., McLaskey, G. C., & Ke, C.-Y. (2020). Groove generation and coalescence on a large-scale laboratory fault. *AGU Advances*, *1*(4), e2020AV000184. https://doi.org/10.1029/2020av000184

Brown, S. R., & Scholz, C. H. (1985). Broad bandwidth study of the topography of natural rock surfaces. *Journal of Geophysical Research*, *90*(B14), 12575–12582. https://doi.org/10.1029/jb090ib14p12575

Brune, J. N. (1970). Tectonic stress and spectra of seismic shear waves from earthquakes. *Journal of Geophysical Research*, *75*(26), 4997–5009. https://doi.org/10.1029/jb075i026p04997

Burridge, R., & Halliday, G. S. (1971). Dynamic shear cracks with friction as models for shallow focus earthquakes. *Geophysical Journal of the Royal Astronomical Society*, *25*(1–3), 261–283. https://doi.org/10.1111/j.1365-246x.1971.tb02339.x

Byerlee, J. D. (1978). Friction of rock. *Pure and Applied Geophysics*, *116*(4–5), 615–626. https://doi.org/10.1007/bf00876528

Candela, T., Renard, F., Klinger, Y., Mair, K., Schmittbuhl, J., & Brodsky, E. E. (2012). Rough-ness of fault surfaces over nine decades of length scales. *Journal of Geophysical ResearchSolid Earth*, *117*(B8). https://doi.org/10.1029/2011jb009041

Cattania, C. (2019). Complex earthquake sequences on simple faults. *Geophysical Research Letters*, *46*(17–18), 10384–10393. https://doi.org/10.1029/2019GL083628

Cattania, C., & Segall, P. (2021). Precursory slow slip and foreshocks on rough faults. *Journal of Geophysical Research: Solid Earth*, *126*(4), e2020JB020430. https://doi.org/10.1029/2020jb020430

Cebry, S. B. L., Ke, C.-Y., & McLaskey, G. C. (2022). The role of background stress state in fluid-induced aseismic slipand dynamic rupture on a 3-m laboratory fault. *Journal of Geophysical Research: Solid Earth*, *127*(8), e2022JB024371. https://doi.org/10.1029/2022jb024371

Cochran, E. S., Page, M. T., van der Elst, N. J., Ross, Z. E., & Trugman, D. T. (2023). Fault roughness at seismogenic depths and links to earthquake behavior. *The Seismic Record*, *3*(1), 37–47. https://doi.org/10.1785/0320220043

Danré, P., Yin, J., Lipovsky, B. P., & Denolle, M. A. (2019). Earthquakeswithin earthquakes: Patterns inrupture complexity. *Geophysical Research Letters*, *46*(13), 7352–7360. https://doi.org/10.1029/2019gl083093

Dempsey, D., & Suckale, J. (2016). Collective properties ofinjection-induced earthquake sequences: 1. Model description and directivity bias. *Journal of Geophysical Research: Solid Earth*, *121*(5), 3609–3637. https://doi.org/10.1002/2015JB012550

Dempsey, D., Suckale, J., & Huang, Y. H. (2016). Collective properties of injection-induced earthquake sequences: 2. Spatiotemporal evolution and magnitude frequency distributions. *Journal of Geophysical Research: Solid Earth*, *121*(5), 3638–3665. https://doi.org/10.1002/2015jb012551

Denolle, M. A., & Shearer, P. M. (2016). New perspectives on self-similarity for shallow thrust earthquakes. *Journal of Geophysical Research: Solid Earth*, *121*(9), 6533–6565. https://doi.org/10.1002/2016jb013105

Dieterich, J. H. (1979). Modeling of rock friction: 1. Experimental results and constitutive equations. *Journal of Geophysical Research*, *84*(B5), 2161–2168. https://doi.org/10.1029/jb084ib05p02161

Dieterich, J. H. (1992). Earthquake nucleation on faults with rate- and state-dependent friction. *Tectonophysics*, *211*(1–4), 115–134. https://doi.org/10.1016/0040-1951(92)90055-b

Dieterich, J. H., & Smith, D. E. (2009). Nonplanar faults: Mechanics of slip and off-fault damage. In *Mechanics, structure and evolution of fault zones* (pp. 1799–1815).

Dodge, D. A., Beroza, G. C., & Ellsworth, W. L. (1995). Foreshock sequence of the 1992 Landers, California, earthquake and its implications for earthquake nucleation. *Journal of Geophysical Research*, *100*(B6), 9865–9880. https://doi.org/10.1029/95jb00871

Dong, P., Xia, K., Xu, Y., Elsworth, D., & Ampuero, J.-P. (2023). Laboratory earthquakes decipher control and stability of rupture speeds. *Nature Communications*, *14*(1), 2427. https://doi.org/10.1038/s41467-023-38137-w

Dunham, E. M., Belanger, D., Cong, L., & Kozdon, J. E. (2011). Earthquake ruptures with strongly rate-weakening friction and off-fault plasticity, Part 2: Nonplanar faults. *Bulletin of the Seismological Society of America*, *101*(5), 2308–2322. https://doi.org/10.1785/0120100076

Fang, Z., & Dunham, E. M. (2013). Additional shear resistance from fault roughness and stress levels on geometrically complex faults. *Journal of Geophysical Research: Solid Earth*, *118*(7), 3642–3654. https://doi.org/10.1002/jgrb.50262

Floyd, M. A., Walters, R. J., Elliott, J. R., Funning, G. J., Svarc, J. L., Murray, J. R., et al. (2016). Spatial variations in fault friction related to lithology from rupture and afterslip of the 2014 South Napa, California, earthquake. *Geophysical Research Letters*, *43*(13), 6808–6816. https://doi.org/10.1002/2016gl069428

Freund, L. B. (1998). *Dynamic fracture mechanics*. Cambridge University Press. Chapter 5.

Gabriel, A.-A., Garagash, D. I., Palgunadi, K. H., & Mai, P. M. (2024). Fault size-dependent fracture energy explains multiscale seismicity and cascading earthquakes. *Science*, *385*(6707), eadj9587. https://doi.org/10.1126/science.adj9587

Gabrieli, T., & Tal, Y. (2025). Lab earthquakes reveal a wide range of rupture behaviors controlled by fault bends. *Proceedings of the National Academy of Sciences*, *122*(17), e2425471122. https://doi.org/10.1073/pnas.2425471122

Goebel, T. H. W., Schorlemmer, D., Becker, T. W., Dresen, G., & Sammis, C. G. (2013). Acoustic emissions document stress changes over many seismic cycles in stick-slip experiments. *Geophysical Research Letters*, *40*(10), 2049–2054. https://doi.org/10.1002/grl.50507

Guglielmi, Y., Cappa, F., Avouac, J., Henry, P., Elsworth, D., Dick, P., & Durand, J. (2015). Seismicity triggered by fluid injection-induced aseismic slip. *Science*, *348*(6240), 1224–1226. https://doi.org/10.1126/science.aab0476

Gulia, L., Tormann, T., Wiemer, S., Herrmann, M., & Seif, S. (2016). Short-term probabilistic earthquake risk assessment considering time-dependent b values. *Geophysical Research Letters*, *43*(3), 1100–1108. https://doi.org/10.1002/2015gl066686

Gulia, L., & Wiemer, S. (2019). Real-time discrimination of earthquake foreshocks and aftershocks. *Nature*, *574*(7777), 193–199. https://doi.org/10.1038/s41586-019-1606-4

Gutenberg, R., & Richter, C. F. (1944). Frequency of earthquakes in California. *Bulletin of the Seismological Society of America*, *34*(4), 185–188. https://doi.org/10.1785/bssa0340040185

Hanks, T. C. (1979). b values and w seismic source models. *Journal of Geophysical Research*, *84*, 2235–2242.

Hanks, T. C., & Kanamori, H. (1979). A moment magnitude scale. *Journal of Geophysical Research*, *84*(B5), 2348–2350. https://doi.org/10.1029/JB084iB05p02348

Harris, R. A., Barall, M., Lockner, D. A., Moore, D. E., Ponce, D. A., Graymer, R. W., et al. (2021). A geology and geodesy based model of dynamic earthquake rupture on the Rodgers creek-hayward-calaveras fault system, California. *Journal of Geophysical Research: Solid Earth*, *126*(3), e2020JB020577. https://doi.org/10.1029/2020jb020577

Heimisson, E. R. (2020). Crack to pulse transition and magnitude statistics during earthquake cycles on a self-similar rough fault. *Earth and Planetary Science Letters*, *537*, 116202. https://doi.org/10.1016/j.epsl.2020.116202

Houston, H. (2001). Influence of depth, focal mechanism, and tectonic setting on the shape and duration of earthquake source time functions. *Journal of Geophysical Research*, *106*(B6), 11137–11150. https://doi.org/10.1029/2000jb900468

Ide, S. (2019). Frequent observations of identical onsets of large and small earthquakes. *Nature*, *573*(7772), 112–116. https://doi.org/10.1038/s41586-019-1508-5

Ide, S., & Aochi, H. (2005). Earthquakes as multiscale dynamic ruptures with heterogeneous fracture surface energy. *Journal of Geophysical Research*, *110*, B11. https://doi.org/10.1029/2004jb003591

Ikari, M., Marone, C., & Saffer, D. (2011). On the relation between fault strength of frictional stability. *Geology*, *39*(1), 83–86. https://doi.org/10.1130/g31416.1

Ito, R., & Kaneko, Y. (2023). Physicalmechanism for a temporal decreaseof the Gutenberg-Richter b-valueprior to a large earthquake. *Journal ofGeophysical Research: Solid Earth*, *128*(12), e2023JB027413. https://doi.org/10.1029/2023jb027413

Kammer, D. S., McLaskey, G. C., Abercrombie, R. E., Ampuero, J.-P., Cattania, C., Cocco, M., et al. (2024). Earthquake energy dissipation in a fracture mechanics framework. *Nature Communications*, *15*(1), 4736. https://doi.org/10.1038/s41467-024-47970-6

Kanamori, H., & Anderson, D. L. (1975). Theoretical basis of some empirical relations in seismology. *Bulletin of the Seismological Society of America*, *65*(5), 1073–1095.

Kato, A., Obara, K., Igarashi, T., Tsuruoka, H., Nakagawa, S., & Hirata, N. (2012). Propagation of slow slip leading up to the 2011 Mw 9.0, Tohoku-Oki earthquake. *Science*, *335*(6069), 705–708. https://doi.org/10.1126/science.1215141

Ke, C.-Y., McLaskey, G. C., & Kammer, D. S. (2018). Rupture termination in laboratory-generated earthquakes. *Geophysical Research Letters*, *45*(23), 12784–12792. https://doi.org/10.1029/2018gl080492

Ke, C.-Y., McLaskey, G. C., & Kammer, D. S. (2021). The earthquake arrest zone. *Geophysical Journal International*, *224*(1), 581–589. https://doi.org/10.1093/gji/ggaa386

Ke, C.-Y., McLaskey, G. C., & Kammer, D. S. (2022). Earthquake breakdown energy scaling despite constant fracture energy. *Nature Communications*, *13*(1), 1005. https://doi.org/10.1038/s41467-022-28647-4

Kwiatek, G., Plenkers, K., & Dresen, G. (2011). Source parameters of picoseismicity recorded at Mponeng Deep Gold Mine, South Africa: Implications for scaling relations. *Bulletin of the Seismological Society of America*, *101*(6), 2592–2608. https://doi.org/10.1785/0120110094

Lee, J., Tsai, V. C., Trugman, D. T., Hirth, G., & Chatterjee, A. (2025). Fault networkgeometry modulates earthquake sourcespectra across scales. *Geophysical Research Letters*, *52*(12), e2025GL115592. https://doi.org/10.1029/2025gl115592

Madariaga, R. (1976). Dynamics of an expanding circular fault. *Bulletin of the Seismological Society of America*, *66*(3), 639–666. https://doi.org/10.1785/bssa0660030639

Manighetti, I., King, G. C. P., Gaudemer, Y., Scholz, C. H., & Doubre, C. (2001). Slip accumulation and lateral propagation of active normal faults in Afar. *Journal of Geophysical Research*, *106*(B7), 13667–13696. https://doi.org/10.1029/2000jb900471

McLaskey, G. (2019). Earthquake initiation from laboratory observations and implications for foreshocks. *Journal of Geophysical Research: Solid Earth*, *124*(12), 12882–12904. https://doi.org/10.1029/2019jb018363

McLaskey, G. C., Kammer, D., & Ke, C.-Y. (2026). Scripts from: Earthquake populations from stochastic stress fields [Dataset]. *Cornell University Library eCommons Repository*. https://doi.org/10.7298/82N3-XD69

McLaskey, G. C., & Lockner, D. A. (2014). Preslip and cascade processes initiating laboratory stick-slip. *Journal of Geophysical Research: Solid Earth*, *119*(8), 6323–6336. https://doi.org/10.1002/2014jb011220

Meier, M. A., Ampuero, J. P., & Heaton, T. H. (2017). The hidden simplicity of subduction megathrust earthquakes. *Science*, *357*(6357), 1277–1281. https://doi.org/10.1126/science.aan5643

Mitchell, T. M., & Faulkner, D. R. (2009). The nature and origin of off-fault damage surrounding strike-slip fault zones with a wide range of displacements: A field study from the Atacama fault system, northern Chile. *Journal of Structural Geology*, *31*(8), 802–816. https://doi.org/10.1016/j.jsg.2009.05.002

Nanjo, K. Z., Hirata, N., Obara, K., & Kasahara, K. (2012). Decade-scale decrease in b value prior to the M9-class 2011 Tohoku and 2004 Sumatra quakes. *Geophysical Research Letters*, *39*(20), L20304. https://doi.org/10.1029/2012gl052997

Nielsen, S., Spagnuolo, E., Violay, M., Smith, S., Di Toro, G., & Bistacchi, A. (2016). G: Fracture energy, friction and dissipation in earthquakes. *Journal of Seismology*, *20*(4), 1187–1205. https://doi.org/10.1007/s10950-016-9560-1

Noda, H., Nakatani, M., & Hori, T. (2013). Large nucleation before large earthquakes is sometimes skipped due to cascade-up—Implications from a rate and state simulation of faults with hierarchical asperities. *Journal of Geophysical Research: Solid Earth*, *118*(6), 2924–2952. https://doi.org/10.1002/jgrb.50211

Ohnaka, M. (2003). A constitutive scaling law and a unified comprehension for frictional slip failure, shear fracture of intact rock, and earthquake rupture. *Journal of Geophysical Research*, *108*(B2), 2080. https://doi.org/10.1029/2000jb000123

Ohnaka, M., & Kuwahara, Y. (1990). Characteristic features of local breakdown near a crack-tip in the transition zone from nucleation to unstable rupture during stick-slip shear failure. *Tectonophysics*, *175*(1–3), 197–220. https://doi.org/10.1016/0040-1951(90)90138-x

Okubo, P. G., & Dieterich, J. H. (1984). Effects of physical fault properties on frictional instabilities produced on simulated faults. *Journal of Geophysical Research*, *89*(B7), 5817–5827. https://doi.org/10.1029/jb089ib07p05817

Oral, E., Ampuero, J. P., Ruiz, J., & Asimaki, D. (2022). A method to generate initial fault stresses for physics-based ground-motion prediction consistent with regional seismicity. *Bulletin of the Seismological Society of America*, *112*(6), 2812–2827. https://doi.org/10.1785/0120220064

Perry, S. M., Lambert, V., & Lapusta, N. (2020). Nearly magnitude-invariant stress drops in simulated crack-like earthquake sequences on rate-and-state faults with thermal pressurization of pore fluids. *Journal of Geophysical Research: Solid Earth*, *125*(3), e2019JB018597. https://doi.org/10.1029/2019jb018597

Power, W. L., Tullis, T. E., Brown, S. R., Boitnott, G. N., & Scholz, C. H. (1987). Roughness of natural fault surfaces. *Geophysical Research Letters*, *14*(1), 29–32. https://doi.org/10.1029/gl014i001p00029

Raleigh, C., Healy, J., & Bredehoeft, J. (1976). An experiment in earthquake control at Rangely, Colorado. *Science*, *191*(4233), 1230–1237. https://doi.org/10.1126/science.191.4233.1230

Renard, F., Voisin, C., Marsan, D., & Schmittbuhl, J. (2006). High resolution 3D laser scanner measurements of a strike-slip fault quantify its morphological anisotropy at all scales. *Geophysical Research Letters*, *33*(4), L04305. https://doi.org/10.1029/2005gl025038

Renou, J., Vallée, M., & Aochi, H. (2022). Deciphering the origins of transient seismic moment accelerations by realistic dynamic rupture simulations. *Bulletin of the Seismological Society of America*.

Ripperger, J., Ampuero, J.-P., Mai, P. M., & Giardini, D. (2007). Earthquake source characteristics from dynamic rupture with constrained stochastic fault stress. *Journal of Geophysical Research*, *112*(B4), B04311. https://doi.org/10.1029/2006jb004515

Rodriguez Padilla, A. M., Oskin, M. E., Brodsky, E. E., Dascher-Cousineau, K., Herrera, V., & White, S. (2024). The Influence of fault geometrical complexity on surface rupture length. *Geophysical Research Letters*, *51*(20), e2024GL109957. https://doi.org/10.1029/2024gl109957

Roeloffs, E. A. (2006). Evidence for aseismic deformation rate changes prior to earthquakes. *Annual Review of Earth and Planetary Sciences*, *34*(1), 591–627. https://doi.org/10.1146/annurev.earth.34.031405.124947

Romanet, P., Saito, T., & Fukuyama, E. (2024). The mechanics of static non-planar faults in infinitesimal strain theory. *Geophysical Journal International*, *239*(3), 1664–1693.

Romanet, P., Sato, D. S., & Ando, R. (2020). Curvature, a mechanical link between the geometrical complexities of a fault: Application to bends, kinks and rough faults. *Geophysical Journal International*, *223*(1), 211–232. https://doi.org/10.1093/gji/ggaa308

Rubin, A. M., & Ampuero, J.-P. (2005). Earthquake nucleation on (aging) rate and state faults. *Journal of Geophysical Research*, *110*(B11), B11312. https://doi.org/10.1029/2005jb003686

Ruina, A. (1983). Slip instability and state variable friction laws. *Journal of Geophysical Research*, *88*(B12), 10359–10370. https://doi.org/10.1029/jb088ib12p10359

Sagy, A., Brodsky, E. E., & Axen, G. J. (2007). Evolution of fault-surface roughness with slip. *Geology*, *35*(3), 283–286. https://doi.org/10.1130/G23235A.1

Scholz, C. H. (1968). The frequency-magnitude relation of microfracturing in rock and its relation to earthquakes. *Bulletin of the Seismological Society of America*, *58*(1), 399–415. https://doi.org/10.1785/bssa0580010399

Shearer, P., Shabikay Senobari, N., & Fialko, Y. (2024). Implications of a reverse polarity earthquake pair on fault friction and stress heterogeneity near Ridgecrest, California. *Journal of Geophysical Research: Solid Earth*, *129*(11), e2024JB029562. https://doi.org/10.1029/2024jb029562

Shi, Z., & Day, S. M. (2013). Rupture dynamics and ground motion from 3-d rough-fault simulations. *Journal of Geophysical Research: Solid Earth*, *118*(3), 1122–1141. https://doi.org/10.1002/jgrb.50094

Sirorattanakul, K., Larochelle, S., Rubino, V., Lapusta, N., & Rosakis, A. J. (2025). Sliding and healing of frictional interfaces that appear stationary. *Nature*, *639*(8056), 947–953. https://doi.org/10.1038/s41586-025-08673-0

Smith, D. E., & Heaton, T. H. (2011). Models of stochastic, spatially varying stress in the crust compatible with focal-mechanism data, and how stress inversions can be biased toward the stress rate. *Bulletin of the Seismological Society of America*, *101*(3), 1396–1421. https://doi.org/10.1785/0120100058

Sone, H., & Uchide, T. (2016). Spatiotemporal evolution of a fault shear stress patch due to viscoelastic interseismic fault zone rheology. *Tectonophysics*, *684*, 63–75. https://doi.org/10.1016/j.tecto.2016.04.017

Svetlizky, I., Kammer, D. S., Bayart, E., Cohen, G., & Fineberg, J. (2017). Brittle fracture theory predicts the equation of motion of frictional rupture fronts. *Physical Review Letters*, *118*(12), 125501. https://doi.org/10.1103/physrevlett.118.125501

Tada, H., Paris, P. C., & Irwin, G. R. (2000). *The stress analysis of cracks handbook edited by 3. Three Park Avenue New York, NY 10016-5990*. ASME. https://doi.org/10.1115/1.801535

Tal, Y., & Hager, B. H. (2018). The slip behavior and source parameters for spontaneous slip events on rough faults subjected to slow tectonic loading. *Journal of Geophysical Research: Solid Earth*, *123*(2), 1810–1823. https://doi.org/10.1002/2017JB014737

Tal, Y., Hager, B. H., & Ampuero, J. P. (2018). The effects of fault roughness on the earthquake nucleation process. *Journal of Geophysical Research: Solid Earth*, *123*(1), 437–456. https://doi.org/10.1002/2017jb014746

Tinti, E., Casarotti, E., Ulrich, T., Taufiqurrahman, T., Li, D., & Gabriel, A.-A. (2021). Constraining families of dynamic models using geological, geodetic and strong ground motion data: The Mw 6.5, October 30th, 2016, Norcia earthquake, Italy. *Earth and Planetary Science Letters*, *576*, 117237. https://doi.org/10.1016/j.epsl.2021.117237

Tormann, T., Wiemer, S., & Mignan, A. (2014). Systematic survey of high-resolution b value imaging along Californian faults: Inference on asperities. *Journal of Geophysical Research: Solid Earth*, *119*(3), 2029–2054. https://doi.org/10.1002/2013jb010867

Uchide, T., & Ide, S. (2010). Scaling of earthquake rupture growth in the Parkfield area: Self-similar growth and suppression by the finite seismogenic layer. *Journal of Geophysical Research*, *115*(B11), B11302. https://doi.org/10.1029/2009jb007122

Uenishi, K., & Rice, J. R. (2003). Universal nucleation length for slip-weakening rupture instability under nonuniform fault loading. *Journal of Geophysical Research*, *108*(B1), 2042. https://doi.org/10.1029/2001JB001681

Ulrich, T., Gabriel, A.-A., Ampuero, J.-P., & Xu, W. (2019). Dynamic viability of the 2016 Mw 7.8 Kaikōura earthquake cascade on weak crustal faults. *Nature Communications*, *10*(1), 1213. https://doi.org/10.1038/s41467-019-09125-w

Venegas-Aravena, P., Crempien, J. G. F., & Archuleta, R. J. (2024). Fractal spatial distributions of initial shear stress and frictional properties on faults and their impact on dynamic earthquake rup-ture. *Bulletin of the Seismological Society of America*, *114*(3), 1444–1465. https://doi.org/10.1785/0120230123

Wise, L., & Tal, Y. (2024). The evolution of stresses and shear resistance on rough faults at large slip. *Tectonophysics*, *880*, 230335. https://doi.org/10.1016/j.tecto.2024.230335

Wong, T.-F. (1986). On the normal stress dependence of the shear fracture energy. In S. Das, J. Boatwright, & C. H. Scholz (Eds.), *Earthquake source mechanics* (pp. 1–11). AGU.

Wu, B. S., & McLaskey, G. C. (2022). Testing earthquake nucleation length scale with Pawnee aftershocks. *Seismological Research Letters*, *93*(4), 2147–2160. https://doi.org/10.1785/0220210184

Yoshida, K., & Kanamori, H. (2023). Time-domain source parameter estimation of Mw 3–7 earthquakes in Japan from a large database of moment-rate functions. *Geophysical Journal International*, *234*(1), 243–262. https://doi.org/10.1093/gji/ggad068